Performance Analysis for User-centric Cell-free Massive MIMO Systems with Hardware Impairments and Multi-antenna Users

Mingfeng Xie, Xiangbin Yu, *Senior Member, IEEE*, Yun Rui, *Senior Member, IEEE*, Kezhi Wang, *Senior Member, IEEE*, Xiaoyu Dang, *Member, IEEE*, and Jiayi Zhang, *Senior Member, IEEE*

***Abstract*—Cell-free massive multiple-input multiple-output (CF mMIMO) is known for its ability to provide ubiquitous connectivity. In this paper, we investigate the achievable spectral efficiency (SE) of a user-centric (UC) CF mMIMO system with both multi-antenna APs and users over joint-correlated Rayleigh fading channels. First, we provide a performance analytical framework for the system with the linear decorrelator and study the impact of hardware impairments (HIs) at transceivers on the uplink SE. Based on that, we discuss the local minimum mean-squared error (MMSE) and partial MMSE combining schemes and the partial large-scale fading decoding (LSFD) method from a scalable point of view. Besides, the exact closed-form SE expression is derived with maximum ratio combining (MRC). Then, we study the MMSE-based successive interference cancelation (MMSE-SIC) detector and give an approximate closed-form SE expression with MRC. In the simulations, we compare the linear decorrelator to the MMSE-SIC detector under different hardware-impaired scenarios. Numerical results correspond to the theoretical analyses and show that the impact of HIs can be mitigated by adding the number of receive antennas.**

***Index Terms*—Hardware impairments, cell-free massive MIMO, spectral efficiency, multi-antenna user, user-centric.**

I. Introduction

In recent years, massive multiple-input multiple-output (MIMO) has been playing an important role in 5G communication networks. It has been successfully applied in Internet of Things [2]–[4] and millimeter-wave communications [5]–[7]. Meanwhile, current trends are suggesting that it has the potential to support other emerging technologies like the reconfigurable intelligent surface [8], integrated sensing and communication [9], and so on. Although researchers have made an effort to enhance the sum rate via an optimal transceiver mode, strong interference may still occur at cell-boundary users, especially in the multicell network [10]. To get ubiquitous and robust connectivity in a future communication network, cell-free massive MIMO (CF mMIMO) is currently deemed as a potential way, which builds an amorphous network [11].

CF mMIMO is integrated with abounding geographically distributed access points (APs) and multiple central processing units (CPUs), handling coordinated multiple points transmission/reception and fronthaul connections in the coverage area [12]. It has been verified that CF mMIMO can provide higher spectral efficiency (SE) and energy efficiency compared to the conventional collocated massive MIMO thanks to a high degree of macro-diversity and low path loss [13], [14]. Except for the elimination of cell boundaries, a natural characteristic of CF mMIMO is its user-centric (UC) essence that users are always served by a certain number of neighboring APs. Based on that, the UC approach is introduced into CF mMIMO where several AP cooperation clusters are pre-defined to communicate with specific users [15]. As discussed in [16], UC CF mMIMO is a special case of scalable CF mMIMO by exploiting the static cooperation cluster, which also accords with the requirements of the scalability issue. Since the properties of channel hardening and favorable propagation are relatively moderate in CF architectures [17], the majority of published papers focused on enhanced signal processing in CF mMIMO systems. The two-layer decoding scheme called the large-scale fading decoding (LSFD) method is considered as an effective decoding technique to deal with interference [18]. It has been applied in the CF mMIMO as two levels of the receiver cooperation at APs and CPUs, making CF mMIMO more flexible in signal processing and more competitive with global or local minimum mean-square error (MMSE) processing [19]–[21], and showing that it is a low-complexity alternative to fully centralized processing. Nevertheless, precoding/combining via MMSE processing is usually with high computational complexity and hard to obtain closed-form analytical expressions. Maximum ratio combining (MRC) is one way that has been extensively researched in systems with the phenomena of channel hardening and favorable propagation. The majority of research in CF mMIMO considered MRC for its simple form and obtainability to closed-form expressions.

A. Related Works

A substantial literature has studied the CF mMIMO systems with single-antenna users nowadays. However, as the

This work is supported in part by National Natural Science Foundation of China (62031017, 61971220, 61971221) and Open Research Fund of State Key Laboratory of Millimeter Waves of Southeast University (K202215). Part of this paper has been presented in IEEE Globecom 2022 [1]. (*Corresponding author: Xiangbin Yu*).

M. Xie, X. Yu, and X. Dang are with College of Electronic and Information Engineering, Nanjing University of Aeronautics and Astronautics, Nanjing, China. X. Yu is also with State Key Lab of Millimeter Waves of Southeast University, China. (Email: xiemf1997@nuaa.edu.cn, yxbxwy@gmail.com, dang@nuaa.edu.cn)

Y. Rui is with the School of Communication and Electronic Engineering, East China Normal University, China. (Email: ruiy@sari.ac.cn)

K. Wang is with Department of Computer Science, Brunel University London, United Kingdom. (Email: kezhi.wang@brunel.ac.uk)

J. Zhang is with the School of Electronic and Information Engineering and the Frontiers Science Center for Smart High-speed Railway System, Beijing Jiaotong University, Beijing, China. (Email: jiayizhang@bjtu.edu.cn).

This article has been accepted for publication in a future issue of this journal, but has not been fully edited. Content may change prior to final publication. Citation information: DOI10.1109/TBC..., IEEE Transactions on Wireless Communications

TABLE I
COMPARISONS OF THE EXISTING WORKS WITH THIS PAPER

Paper	Multi-antenna user	Joint correlation	Scalability	SINR analysis	MMSE-SIC	LSFD	Additive Distortions
[26]	✓	✗	✗	✓	✗	✗	✗
[29], [30]	✓	✗	✗	✗	✓	✗	✗
[31], [32]	✓	✓	✗	✗	✓	✓	✗
[38], [39]	✗	✗	✗	✓	✗	✓	✓
[44]	✗	✗	✓	✓	✗	✗	✓
Current work	✓	✓	✓	✓	✓	✓	✓

dimension of the antenna array increases, it is necessary to investigate multi-antenna equipment for the obtainable spatial multiplexing gains, which has been proven efficient and effective in a massive MIMO system [22]–[24]. The authors in [25] investigated the UC CF mMIMO with multi-antenna nodes at millimeter wave frequencies, where both downlink (DL) and uplink (UL) sum SE were maximized via the proposed power allocation algorithm. Instead of applying the MMSE-based successive interference cancellation (MMSE-SIC) detector above, the authors in [26] utilized a linear combining scheme to detect each data stream transmitted through each transmit antenna independently, announcing that additional antennas at users improved the system's SE. Further, the authors in [27] found that the UC approach generally outperformed the CF approach wherein multi-antenna nodes were presumed, especially during the UL transmission. The authors in [28] studied the effect of DL pilot transmission on the DL SE of CF mMIMO with multi-antenna users, indicating that DL training had higher channel estimation quality but higher estimation overhead. The authors in [29] and [30] investigated the impact of multi-antenna users and low-resolution quantization on the multigroup multicast CF mMIMO with conjugate beamforming receivers, where a closed-form expression of the DL SE was derived. Nevertheless, none of the aforementioned works have paid attention to the impact of jointly spatial correlation brought by multi-antenna APs and multi-antenna users. In the latest research of multi-antenna users in CF mMIMO systems [31], [32], the complete spatial correlation channel model has been given to investigate four different UL implementations, from fully centralized to fully distributed. The ideal hardware was assumed at the expense of unexpectedly high costs.

Hardware impairments (HIs) have been comprehensively investigated in massive MIMO systems, which model different hardware components as addition or multiplicative distortions, e.g., amplifier non-linearities, amplitude/phase imbalance, phase noise, and finite-resolution quantization [33]–[37]. The authors in [38] first introduced the generic modeling of additive distortions into CF mMIMO systems, and they further investigated the impact of different LSFD coefficients in [39]. The authors in [40], [41] considered a CF mMIMO system with low-resolution quantization, suggesting that employing more antennas could mitigate the effect of quantization noise at the APs. In [42], the authors studied three transmission strategies at APs with limited capacity fronthauls under HIs and proposed low-complexity fronthaul rate allocations. Particularly, the authors in [43] studied the effect of power amplifier non-linearity and found that the UL transmission was more sensitive to non-linearity than the DL transmission. In [44], the authors further spotlighted the impact of amplified thermal noise and phase noise in the local oscillators along with the additive impairments. Note that they only considered the single-antenna-user scenario. In a nutshell, low-cost hardware is more attractive than high-precision hardware to establish an economical-efficient network, which makes analyses on HIs critical. To the best of our knowledge, very few researchers have ever studied the impact of element-uncorrelated hardware distortions on the jointly spatial-correlated MIMO channels in CF systems. The comparisons between our work and existing works are summarized in Table I with major contributions listed as follows.

B. Contributions

Motivated by the above observations, we introduce the generic model for the aggregate impact of transceiver HIs in [37] into a UC CF mMIMO system with both multi-antenna APs and multi-antenna users in this paper. The classic Kronecker channel model [45] is adopted here to describe joint-correlated Rayleigh fading channels in an urban and crowded scenario.

- We employ the UC approach and the LSFD method in the CF mMIMO system and provide the performance analytical framework of the linear decorrelator which detects each data stream individually [46]. Based on the signal-to-interference-and-noise ratio (SINR) derived via the use-and-then-forget (UatF) bound, we provide the achievable UL SE expression which holds for arbitrary linear combiners. Specifically, the exact closed-form UL SE expression is derived with MRC.
- As a comparison, we provide the performance analytical framework of the MMSE-SIC detector with arbitrary linear combiners. The optimal LSFD coefficient matrix is given under HIs with expectations retained. Based on MRC, an approximate closed-form SE expression of the MMSE-SIC detector is derived along with the suboptimal LSFD coefficient matrix, which turns into an exact expression with ideal hardware.
- We shed light on the local MMSE and partial MMSE (PMMSE) combining schemes to show that the local PMMSE combining scheme can be a scalable alternative combiner. Furthermore, we investigate the impact of the hardware distortion correlation and the different LSFD coefficients on the achievable UL SE. Finally, numerical results are presented to validate the theoretical analyses. We show that the hardware-quality scaling law complements the performance loss resulting from HIs by adding the number of receive antennas.

This article has been accepted for publication in a future issue of this journal, but has not been fully edited. Content may change prior to final publication. Citation information: DOI10.1109/TBC..., IEEE Transactions on Wireless Communications

TABLE II
LIST OF ACRONYMS

Acronym	Definition
AP	Access point
CDF	Cumulative distribution function
CF mMIMO	Cell-free massive multiple-input multiple-output
CPU	Central processing unit
DL/UL	Downlink/Uplink
HI	Hardware impairment
(L/P)MMSE	(Linear/Partial) Minimum mean-square error
(P)LSFD	(Partial) Large-scale fading decoding
MIMO	Multiple-input multiple-output
MMSE-SIC	Minimum-mean-square-error-based successive interference cancellation
MRC	Maximum ratio combining
S-CD/S-LSFD	Simple centralized decoding/Simple large-scale fading decoding
SE	Spectral efficiency
SINR	Signal-to-interference-and-noise ratio
UatF	Use-and-then-forget
UC	User-centric

In order to improve the flow of this paper, we provide the list of acronyms in Table II. Note that a channel estimation scheme with the single-radio-frequency chain was investigated in the conference version [1] under this hardware-impaired and spatial-correlated CF mMIMO system with multi-antenna users, where we compared the normalized mean-square error and the computational complexity. Based on that, we utilize the UC approach and the results of the channel estimation scheme with full-radio-frequency chains to study the UL transmission and derive the SE expressions of the linear decorrelator and the MMSE-SIC detector in this paper.

C. Outline

The organization of the remainder of this paper is as follows: Section II presents the system model of the UC CF mMIMO system with joint correlation and HIs. Section III and Section IV present the analytical frameworks of the achievable SE with the linear decorrelator and the MMSE-SIC detector, respectively. The closed-form expressions of the achievable SE are also given in these sections with MRC and LSFD, and the hardware distortion correlation is specifically discussed in Section III. In Section V, the simulation results are presented to validate our analytical results and insights. Finally, conclusions and outlooks are drawn in Section VI.

D. Notations

$(\cdot)^{-1}$, $(\cdot)^*$, $(\cdot)^T$, and $(\cdot)^H$ stand for inverse, conjugate, transpose, and conjugate transpose, respectively. Boldface lowercase letter $\mathbf{x}$ and boldface uppercase letter $\mathbf{X}$ denote column vector and matrix. The n-th column of $\mathbf{X}$ is denoted by $\mathbf{x}_n$, and the (m,n)-th element of $\mathbf{X}$ is denoted by x_{mn}. $\mathbb{E}\{\cdot\}$, $\mathrm{tr}(\cdot)$, $\mathrm{diag}(\cdot)$, $\mathrm{blkdiag}(\cdot)$, and $\mathrm{vec}(\cdot)$ represent the expectation, trace, diagonalization, block diagonalization, and vectorization operator, respectively. The determinant of a matrix is denoted as $\det(\cdot)$, and $\mathbf{I}_P$, $\mathbf{0}^{M\times N}$ and $\mathbf{1}^{M\times N}$ are a P-dimension identity matrix, and $M \times N$ matrices with zero and unit entries. $|\cdot|$ and $\|\cdot\|$ denote the absolute value and the Frobenius norm. $\otimes$ and $\odot$ denote the Kronecker and element-wise product. $\mathbf{x} \sim \mathcal{CN}(\mathbf{0}, \mathbf{R})$ represents a complex Gaussian random vector with correlation matrix $\mathbf{R}$, and the correlation matrix of a random matrix is defined as the counterpart of its vectorized version.

II. SYSTEM MODEL

We consider a CF mMIMO system shown in Fig. 1 with L APs and K users uniformly distributed over a geographic area, where multiple antennas are equipped at both APs and users. M and N represent the number of antennas per AP and per user with full radio-frequency chains, respectively. The fronthaul network is assumed ideal in this paper, where the error-free and capacity-unlimited optical fiber fronthauls are assumed. We consider two receiver architectures where the linear decorrelator is low-complexity and efficient but may bring about performance loss due to the uncorrelations of detection between different data streams. Another effective per-user-basis detector for multi-antenna users is the MMSE-SIC detector, which incorporates the SIC into the linear decorrelator with the MMSE receiver and has been proven optimal to achieve the best possible sum rate over Rayleigh fading channels. Note that these two detectors share the same local channel estimates.

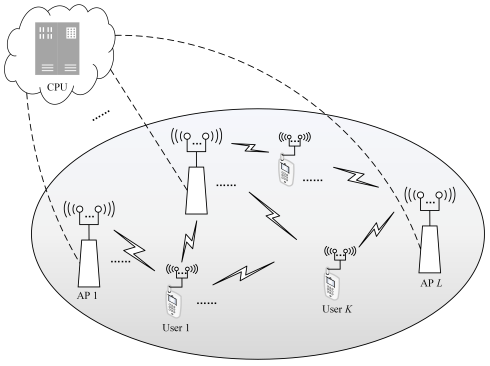

Fig. 1. A CF mMIMO network model with multi-antenna nodes.

A. Channel Model

The standard block fading model is adopted under the time division duplex mode, operating in the same time-frequency resources. The channel impulse responses are assumed constant in a coherence block of τ_c length which is divided into the training duration τ_p and the data transmission $\tau_u = \tau_c - \tau_p$. Due to the multi-antenna architectures, both transmit and receive spatial correlations cannot be neglected. Thus, we introduce the conventional Kronecker model to describe the joint-correlated Rayleigh channel matrix from user k to AP l as $\mathbf{G}_{lk} = \left(\mathbf{R}_{lk,\mathrm{r}}\right)^{1/2} \mathbf{H}_{lk} \left(\mathbf{R}_{k,\mathrm{t}}\right)^{T/2}$, where $\mathbf{H}_{lk} \in \mathbb{C}^{M\times N}$ is the small-scale fading matrix whose elements follow independently and identically distributed (i.i.d) $\mathcal{CN}(0,1)$. According to [45], the (i,j)-th element in transmit spatial correlation matrix $\mathbf{R}_{k,\mathrm{t}} \in \mathbb{R}^{N\times N}$ of user k can be computed by Jakes' model as $r_{k,\mathrm{t},ij} = J_0\left(2\pi d_k |i-j|/\lambda\right)$, where $J_0(\cdot)$ denotes the zero-order Bessel function of the first kind, d_k is the distance between the adjacent antennas of user k, and λ is the carrier wavelength. The positive semi-definite receive spatial correlation matrix $\mathbf{R}_{lk,\mathrm{r}} \in \mathbb{C}^{M\times M}$

This article has been accepted for publication in a future issue of this journal, but has not been fully edited. Content may change prior to final publication. Citation information: DOI10.1109/TBC..., IEEE Transactions on Wireless Communications

is defined in [47, Sec. 2.5.3] where the large-scale fading coefficient $\beta_{lk} = \mathrm{tr}\left(\mathbf{R}_{lk,\mathrm{r}}\right)/M$. Thus, the joint correlation matrix is denoted as $\mathbf{R}_{lk} = \mathbf{R}_{k,\mathrm{t}} \otimes \mathbf{R}_{lk,\mathrm{r}}$, from which we can further obtain $\mathbf{G}_{lk} \sim \mathcal{CN}(\mathbf{0}, \mathbf{R}_{lk})$ and the vectorization version $\mathbf{g}_{lk} = \mathrm{vec}(\mathbf{G}_{lk}) = \left(\mathbf{R}_{k,\mathrm{t}}^{1/2} \otimes \mathbf{R}_{lk,\mathrm{r}}^{1/2}\right)\mathrm{vec}(\mathbf{H}_{lk})$. We define $\mathbf{S}_n = \left[\mathbf{0}^{N\times M(n-1)}, \mathbf{I}_M, \mathbf{0}^{N\times M(N-n)}\right]$ so that the channel from transmit antenna n at user k to AP l is denoted as $\mathbf{g}_{lkn} = \mathbf{S}_n\mathbf{g}_{lk}$. For convenience, we assume the transmit and receive spatial correlation matrices are both available via methods in [48]–[52] when in demand.

B. Uplink Data Transmission

In the UC approach, we denote the set of APs serving user k as $\mathcal{L}_k$. Given the set $\mathcal{L}_k$ for $k = 1, \cdots, K$, we can get the set of users served by AP l as $\mathcal{K}_l$. To provide a generic model, we introduce a set of diagonal matrices $\mathbf{D}_{lk}$, which is described in [47] and defined as $\mathbf{D}_{lk} = \mathbf{I}_M$ when $l \in \mathcal{L}_k$ and $\mathbf{0}^{M\times M}$ when $l \notin \mathcal{L}_k$.

The signal of multiple data streams transmitted by user k is denoted as $\mathbf{s}_k = [s_{k1}, \cdots, s_{kN}]^T$ with $s_{kn} \sim \mathcal{CN}(0,1)$. The power control matrix for user k is $\mathbf{P}_k = p_k\,\mathrm{diag}(\xi_{k1}, \cdots, \xi_{kN})$, where p_k is the maximum transmit power of user k, and $\xi_{kn} \in [0,1]$ is the power control factor of transmit antenna n. Assuming the hardware quality of each transmit antenna or receive antenna is identical [35]–[39], the received signal passing through the hardware-impaired transceiver at AP l can be expressed as

$$\mathbf{y}_l = \sqrt{\kappa_{l,\mathrm{r}}}\sum_{i=1}^{K}\mathbf{G}_{li}\left(\sqrt{\kappa_{i,\mathrm{t}}}\mathbf{P}_i^{1/2}\mathbf{s}_i + \boldsymbol{\eta}_{i,\mathrm{t}}\right) + \boldsymbol{\eta}_{l,\mathrm{r}} + \mathbf{w}_l, \tag{1}$$

where $0 < \kappa_{i,\mathrm{t}}, \kappa_{l,\mathrm{r}} \le 1$ are the hardware quality factors of the transmitter and receiver, and $\mathbf{w}_l$ is the additive thermal noise at the receiver with elements following i.i.d. $\mathcal{CN}(0,\sigma^2)$. The hardware quality factors are assumed to be the same for all users and APs, respectively (i.e., $\kappa_{i,\mathrm{t}} = \kappa_{\mathrm{t}}$ and $\kappa_{l,\mathrm{r}} = \kappa_{\mathrm{r}}$). The transmitter distortion $\boldsymbol{\eta}_{k,\mathrm{t}} \in \mathbb{C}^{N\times 1}$ at user k subjects to $\mathcal{CN}(\mathbf{0}, (1-\kappa_{\mathrm{t}})\mathbf{P}_k)$. The receiver distortion $\boldsymbol{\eta}_{l,\mathrm{r}} \in \mathbb{C}^{M\times 1}$ at AP l follows $\mathcal{CN}(\mathbf{0}, \mathbf{C}_{l|\mathbf{G}})$, where the conditional covariance is expressed as $\mathbf{C}_{l|\mathbf{G}} = (1-\kappa_{\mathrm{r}})\sum_{k=1}^{K}\mathbf{G}_{lk}\mathbf{P}_k\mathbf{G}_{lk}^H \odot \mathbf{I}_M$. The off-diagonal elements are zero due to the uncorrelations of the receive distortions between different receive antennas. The unconditional distribution of $\boldsymbol{\eta}_{l,\mathrm{r}}$ can be expressed as $\boldsymbol{\eta}_{l,\mathrm{r}} = \sum_{k=1}^{K}\sum_{n=1}^{N}\sqrt{p_k\xi_{kn}(1-\kappa_{\mathrm{r}})}\mathbf{g}_{lkn} \odot \bar{\boldsymbol{\eta}}_{lkn}$, where $\bar{\boldsymbol{\eta}}_{lkn} \sim \mathcal{CN}(\mathbf{0}, \mathbf{I}_M)$ and is i.i.d. for $\forall l, k, n$ [37].

C. Pilot Transmission

Regular pilot transmission is considered, where users transmit multiple data streams of pilot sequences through all transmit antennas simultaneously. Each user transmits the pilot matrix $\boldsymbol{\Phi}_k = [\boldsymbol{\phi}_{k1}, \cdots, \boldsymbol{\phi}_{kN}]$, whose columns are picked out from τ_p pairwisely orthogonal pilot sequences $\boldsymbol{\phi}_t \in \mathbb{C}^{\tau_p\times 1}$ for $t = 1, \cdots, \tau_p$ with $\|\boldsymbol{\phi}_t\|^2 = 1$.

During the uplink training, the received signal of AP l through distortions is expressed as

$$\mathbf{Y}_l^{\mathrm{p}} = \sqrt{\kappa_{\mathrm{r}}}\sum_{k=1}^{K}\mathbf{G}_{lk}\left(\sqrt{\tau_p\kappa_{\mathrm{t}}}\boldsymbol{\Phi}_k\mathbf{P}_k^{1/2} + \boldsymbol{\Pi}_{k,\mathrm{t}}\right)^H + \boldsymbol{\Pi}_{l,\mathrm{r}} + \mathbf{W}_l, \tag{2}$$

where $\mathbf{W}_l \sim \mathcal{CN}(\mathbf{0}, \sigma^2\mathbf{I}_{M\tau_p})$ is additive thermal noise. The transmitter and receiver distortions $\boldsymbol{\Pi}_{k,\mathrm{t}} \in \mathbb{C}^{\tau_p\times N}$ and $\boldsymbol{\Pi}_{l,\mathrm{r}} \in \mathbb{C}^{M\times\tau_p}$ are distributed as $\mathcal{CN}(\mathbf{0}, (1-\kappa_{\mathrm{t}})\mathbf{P}_k \otimes \mathbf{I}_{\tau_p})$ and $\mathcal{CN}(\mathbf{0}, \mathbf{C}_{l|\mathbf{G}}^{\mathrm{p}})$, respectively. The conditional covariance of $\boldsymbol{\Pi}_{l,\mathrm{r}}$ is $\mathbf{C}_{l|\mathbf{G}}^{\mathrm{p}} = \mathbf{I}_{\tau_p} \otimes \mathbf{C}_{l|\mathbf{G}}$, indicating that each column in $\boldsymbol{\Pi}_{l,\mathrm{r}}$ is i.i.d. as $\boldsymbol{\eta}_{l,\mathrm{r}}$. Additionally, the unconditional distribution of $\boldsymbol{\Pi}_{l,\mathrm{r}}$ can be expressed as

$$\boldsymbol{\Pi}_{l,\mathrm{r}} = \sqrt{1-\kappa_{\mathrm{r}}}\sum_{k=1}^{K}\left(\left(\mathbf{1}^{1\times\tau_p} \otimes \mathbf{G}_{lk}\right) \odot \breve{\boldsymbol{\Pi}}_{lk}\right)\bar{\mathbf{P}}_k, \tag{3}$$

where the elements in $\breve{\boldsymbol{\Pi}}_{lk} \in \mathbb{C}^{M\times N\tau_p}$ follow i.i.d. $\mathcal{CN}(0,1)$ and $\bar{\mathbf{P}}_k = \mathbf{I}_{\tau_p} \otimes \mathbf{P}_k^{1/2}\mathbf{1}^{N\times 1}$.

III. Uplink SE Analysis of Linear Decorrelator

In this section, we specifically investigate the achievable UL SE of the linear decorrelator. To meet the requirements of scalability, we only pay attention to "Level 3" and "Level 2" in [16]. The discussions of "Level 4" and "Level 1" are omitted for "Level 4" possesses extremely high complexity, and "Level 1" (i.e., small cell network) cannot mitigate the co-channel interference in a high-user-density scenario.

A. Pilot Assignment and Channel Estimation

Random pilot assignment is one of the effective schemes to assign pilot sequences to users in the single-antenna scenario regardless of any side information. However, it is not applicable in the multi-antenna-user scenario in that there might exist identical columns in $\boldsymbol{\Phi}_k$ without proper designs, giving rise to both intra-user and inter-user pilot contaminations. The intra-user pilot reuse may magnify the effect of additive noise. The researchers instinctively defined the assigned pilot matrices as $\boldsymbol{\Phi}_{k'}^H\boldsymbol{\Phi}_k = \mathbf{I}_N$ if the same pilot matrix was assigned to both user k' and user k, and $\boldsymbol{\Phi}_{k'}^H\boldsymbol{\Phi}_k = \mathbf{0}^{N\times N}$ otherwise [25]–[31]. It has to make sure that τ_p is an integer multiple of N, otherwise $\tau_p - \lfloor\tau_p/N\rfloor$ orthogonal pilot sequences would be wasted.

To avoid intra-user pilot contaminations and limitations on τ_p, we generalize the random pilot assignment to multi-antenna-user cases via its counterpart in the multicell massive MIMO network [54]. Assuming $\tau_p \ge N$, the pilot matrix of each user is formed by N distinct pilot sequences, which are selected randomly out of τ_p pairwisely orthogonal pilot sequences. Accordingly, intra-user pilot contaminations are eliminated, and there are no other restrictions on τ_p. Notice that inter-user pilot contaminations happen partially because users are probable to reuse less than N pilot sequences. Concretely, we have $\boldsymbol{\Phi}_{k'}^H\boldsymbol{\Phi}_k = \bar{\boldsymbol{\Phi}}_{k'k}$, where the (n',n)-th element in $\bar{\boldsymbol{\Phi}}_{k'k}$ is 1 if $\boldsymbol{\phi}_{k'n'} = \boldsymbol{\phi}_{kn}$ and 0 otherwise.

After receiving the pilot signal in (2), the despreading operation is performed that $\mathbf{Y}_{lk}^{\mathrm{p}} = \mathbf{Y}_l^{\mathrm{p}}\boldsymbol{\Phi}_k$. Then, we can obtain the linear MMSE (LMMSE) channel estimate of user k at AP l in the form of vectorization.

Theorem 1. *The LMMSE estimate of* $\mathbf{G}_{lk}$ *is given by*

$$\hat{\mathbf{g}}_{lk} = \mathrm{vec}\left(\hat{\mathbf{G}}_{lk}\right) = \mathbf{C}_{lk,\mathbf{GY}}\mathbf{C}_{lk,\mathbf{Y}}^{-1}\mathbf{y}_{lk}^{\mathrm{p}} = \boldsymbol{\Psi}_{lk}\mathbf{y}_{lk}^{\mathrm{p}}, \tag{4}$$

where $\mathbf{y}_{lk}^{\mathrm{p}} = \mathrm{vec}\left(\mathbf{Y}_{lk}^{\mathrm{p}}\right)$ *and* $\mathbf{C}_{lk,\mathbf{GY}} = \sqrt{\tau_p\kappa_{\mathrm{t}}\kappa_{\mathrm{r}}}\mathbf{R}_{lk,\mathrm{t}}\mathbf{P}_k^{1/2}\bar{\boldsymbol{\Phi}}_{kk}^* \otimes \mathbf{R}_{lk,\mathrm{r}}$. $\mathbf{C}_{lk,\mathbf{Y}}$ *is shown as (5) at the top of the next page, where*

$$\mathbf{C}_{lk,\mathbf{Y}} = \tau_p \kappa_{\mathrm{t}} \kappa_{\mathrm{r}} \sum_{k'=1}^{K} \bar{\mathbf{\Phi}}_{k'k}^{T} \mathbf{P}_{k'}^{1/2} \mathbf{R}_{lk,\mathrm{t}} \mathbf{P}_{k'}^{1/2} \bar{\mathbf{\Phi}}_{k'k}^{*} \otimes \mathbf{R}_{lk,\mathrm{r}} + \sigma^2 \bar{\mathbf{\Phi}}_{kk}^{T} \otimes \mathbf{I}_M + \sum_{k'=1}^{K} \bar{\mathbf{\Phi}}_{kk}^{T} \otimes (\kappa_{\mathrm{r}}(1-\kappa_{\mathrm{t}}) \mathbf{Z}_{lk'} + (1-\kappa_{\mathrm{r}}) \mathbf{Z}_{lk'} \odot \mathbf{I}_M) \quad (5)$$

$$\mathrm{SINR}_{kn} = \frac{p_k \xi_{kn} \left| \sum_{l=1}^{L} a_{lkn}^{*} \mathrm{A}_{lkn} \right|^2}{\sum_{k'=1}^{K} \sum_{n'=1}^{N} \frac{p_{k'} \xi_{k'n'}}{\kappa_{\mathrm{t}}} \left(\mathrm{B}_{knk'n'} + \frac{1-\kappa_{\mathrm{r}}}{\kappa_{\mathrm{r}}} \sum_{l=1}^{L} |a_{lkn}|^2 \mathrm{C}_{lknk'n'} \right) - p_k \xi_{kn} \left| \sum_{l=1}^{L} a_{lkn}^{*} \mathrm{A}_{lkn} \right|^2 + \frac{\sigma^2}{\kappa_{\mathrm{t}} \kappa_{\mathrm{r}}} \sum_{l=1}^{L} |a_{lkn}|^2 \mathrm{D}_{lkn}} \quad (7)$$

$\mathbf{Z}_{lk} = \sum_{n=1}^{N} p_k \xi_{kn} \mathbf{R}_{lk,\mathrm{r}}$.

Proof: Please refer to our conference version [1]. ∎

The covariance of the channel estimate $\hat{\mathbf{G}}_{lk}$ is $\hat{\mathbf{R}}_{lk} = \mathbf{C}_{lk,\mathbf{GY}} \mathbf{C}_{lk,\mathbf{Y}}^{-1} \mathbf{C}_{lk,\mathbf{GY}}^{H}$, and that of the estimation error $\tilde{\mathbf{G}}_{lk} = \mathbf{G}_{lk} - \hat{\mathbf{G}}_{lk}$ is $\tilde{\mathbf{R}}_{lk} = \mathbf{R}_{lk} - \hat{\mathbf{R}}_{lk}$. Note that $\tilde{\mathbf{G}}_{lk}$ is uncorrelated but not independent from $\hat{\mathbf{G}}_{lk}$ for the non-Gaussian nature of the channel estimates.

B. Generic SE Expressions

We suppose that the decorrelation between different antenna elements is successful. Hence, the corresponding SINR for each antenna equipped at users can be computed separately. In this case, we give the analyses on the SINR.

In the first stage of the LSFD method, each AP performs local detection for each user with local channel estimates, and the local estimate of the substream symbol s_{kn} is combined as $\hat{s}_{lkn} = \mathbf{v}_{lkn}^{H} \mathbf{D}_{lk} \mathbf{y}_l$. Note that the local estimates would not be computed for $\mathbf{D}_{lk} = \mathbf{0}^{M \times M}$. In the second stage, the final detection of s_{kn} at the CPU is a weighted sum of local estimates from all APs serving user k, which is expressed as

$$\begin{aligned} \tilde{s}_{kn} = & \sum_{l=1}^{L} \sum_{k'=1}^{K} \sum_{n'=1}^{N} a_{lkn}^{*} \sqrt{\kappa_{\mathrm{t}} \kappa_{\mathrm{r}} p_{k'} \xi_{k'n'}} \mathbf{v}_{lkn}^{H} \mathbf{D}_{lk} \mathbf{g}_{lk'n'} s_{k'n'} \\ & + \sqrt{\kappa_{\mathrm{r}}} \sum_{l=1}^{L} \sum_{k'=1}^{K} a_{lkn}^{*} \mathbf{v}_{lkn}^{H} \mathbf{D}_{lk} \mathbf{G}_{lk'} \boldsymbol{\eta}_{k',\mathrm{t}} \\ & + \sum_{l=1}^{L} a_{lkn}^{*} \mathbf{v}_{lkn}^{H} \mathbf{D}_{lk} \boldsymbol{\eta}_{l,\mathrm{r}} + \sum_{l=1}^{L} a_{lkn}^{*} \mathbf{v}_{lkn}^{H} \mathbf{D}_{lk} \mathbf{n}_l, \end{aligned} \quad (6)$$

where $\mathbf{a}_{kn} = [a_{1kn}, \cdots, a_{Lkn}]^T$ contains the LSFD coefficients depending on the large-scale fading information, and $\mathbf{v}_{lkn}$ is the n-th column of the local combining matrix $\mathbf{V}_{lk}$.

Corollary 1. *The achievable UL SE of substream n for user k is expressed as* $\mathrm{SE}_{kn} = (1 - \tau_p/\tau_c) \log_2(1 + \mathrm{SINR}_{kn})$*, where* SINR_{kn} *is given in (7) at the top of this page, and corresponding terms are expressed as* $\mathrm{A}_{lkn} = \mathbb{E}\{\mathbf{v}_{lkn}^{H} \mathbf{D}_{lk} \mathbf{g}_{lkn}\}$, $\mathrm{B}_{knk'n'} = \mathbb{E}\{|\sum_{l=1}^{L} a_{lkn}^{*} \mathbf{v}_{lkn}^{H} \mathbf{D}_{lk} \mathbf{g}_{lk'n'}|^2\}$, $\mathrm{C}_{lknk'n'} = \mathbb{E}\{\|\mathbf{D}_{lk} \mathbf{v}_{lkn} \odot \mathbf{g}_{lk'n'}\|^2\}$, *and* $\mathrm{D}_{lkn} = \mathbb{E}\{\|\mathbf{D}_{lk} \mathbf{v}_{lkn}\|^2\}$*, respectively.*

Proof: It follows similar procedures in [37, Theorem 4.4.] and [47, Theorem 5.4.] and is accordingly omitted. ∎

Corollary 2. *The achievable UL SE of substream n for user k is maximized by*

$$\mathbf{a}_{kn} = \left(\sum_{k'=1}^{K} \sum_{n'=1}^{N} \mathbb{E}\left\{ \mathbf{b}_{knk'n'} \mathbf{b}_{knk'n'}^{H} \right\} + \frac{1}{\kappa_{\mathrm{r}}} \mathbf{F}_{kn} \right)^{-1} \mathbb{E}\left\{ \mathbf{b}_{knkn} \right\}, \quad (8)$$

where $\mathbf{F}_{kn} = \mathrm{diag}(f_{1kn}, \cdots, f_{Lkn})$, $\mathbf{b}_{knk'n'} = [b_{knk'n',1}, \cdots, b_{knk'n',L}]^T$, *and the elements in them are* $f_{lkn} = \sigma^2 \mathbb{E}\{\|\mathbf{D}_{lk} \mathbf{v}_{lkn}\|^2\} + (1 - \kappa_{\mathrm{r}}) \sum_{k'=1}^{K} \sum_{n'=1}^{N} p_{k'} \xi_{k'n'} \mathbb{E}\{\|\mathbf{D}_{lk} \mathbf{v}_{lkn} \odot \mathbf{g}_{lk'n'}\|^2\}$ *and* $b_{knk'n',l} = \sqrt{p_{k'} \xi_{k'n'}} \mathbf{v}_{lkn}^{H} \mathbf{D}_{lk} \mathbf{g}_{lk'n'}$*, respectively. The maximized SINR value is shown as (9) at the top of the next page.*

Proof: It can be derived with the maximization generalized Rayleigh quotient. ∎

To reduce the complexity of LSFD and motivated by [55], the partial LSFD (PLSFD) scheme is applied here by introducing $\mathbf{D}_{lk'}$ into $\mathbf{b}_{knk'n'}$ and f_{lkn}. The elements in the novel $\tilde{\mathbf{b}}_{knk'n'}$ and $\tilde{\mathbf{F}}_{kn}$ are respectively expressed as $\tilde{b}_{knk'n',l} = \mathbf{v}_{lkn}^{H} \mathbf{D}_{lk,k'} \mathbf{g}_{lk'n'}$ and $\tilde{f}_{lkn} = \sigma^2 \mathbb{E}\{\|\mathbf{D}_{lk,k'} \mathbf{v}_{lkn}\|^2\} + (1 - \kappa_{\mathrm{r}}) \sum_{k'=1}^{K} \sum_{n'=1}^{N} p_{k'} \xi_{k'n'} \mathbb{E}\{\|\mathbf{D}_{lk,k'} \mathbf{v}_{lkn} \odot \mathbf{g}_{lk'n'}\|^2\}$, where $\mathbf{D}_{lk,k'} = \mathbf{D}_{lk} \mathbf{D}_{lk'}$. The PLSFD coefficients are calculated only for $\mathbf{D}_{lk,k'} \neq \mathbf{0}^{M \times M}$, which is a scalable strategy.

Remark 1. *Two more efficient methods to reduce the computational complexity are simple centralized decoding (S-CD) that* $\mathbf{a}_{kn} = [1/L, \cdots, 1/L]^T$ *and simple LSFD (S-LSFD) that* $\mathbf{a}_{kn} = [\beta_{1k}/\sum_{k'=1}^{K} \beta_{1k'}, \cdots, \beta_{Lk}/\sum_{k'=1}^{K} \beta_{Lk'}]^T$ *[39]. Generalized to the scalable version, the l-th element S-LSFD can be calculated in terms of its serving cluster as* $\beta_{lk}/\sum_{k' \in \mathcal{K}_l} \beta_{lk'}$ *for* $\mathbf{D}_{lk} = \mathbf{I}_M$*. The performance loss is inevitable when exploiting these simple combinations at the CPU, but the computational complexity is remarkably reduced.*

Since (7) holds for arbitrary linear combiners, we study three linear combiners using local channel estimates. The simplest one is MRC that $\mathbf{v}_{lkn} = \hat{\mathbf{g}}_{lkn}$, which is used to derive closed-form expressions of the achievable SE. Another one that reaches higher performance is the local MMSE combiner. It appears more complicated than MRC and can be expressed as

$$\mathbf{V}_{lk} = \sqrt{\kappa_{\mathrm{t}} \kappa_{\mathrm{r}}} \left(\sum_{k'=1}^{K} \hat{\mathbf{G}}_{lk'} \mathbf{P}_{k'} \hat{\mathbf{G}}_{lk'}^{H} \odot \mathbf{E}_1 + \mathbf{C}_{lk'} + \sigma^2 \mathbf{I}_M \right)^{-1} \hat{\mathbf{G}}_{lk} \mathbf{P}_{k}^{1/2}, \quad (10)$$

where the constant matrix $\mathbf{E}_1 = \kappa_{\mathrm{r}} \mathbf{1}^{M \times M} + (1 - \kappa_{\mathrm{r}}) \mathbf{I}_M$ and $\mathbf{C}_{lk'} = \mathbb{E}\left\{ \tilde{\mathbf{G}}_{lk'} \mathbf{P}_{k'} \tilde{\mathbf{G}}_{lk'}^{H} \right\} \odot \mathbf{E}_1 = \sum_{n=1}^{N} p_{k'} \xi_{k'n} \mathbf{S}_n \tilde{\mathbf{R}}_{lk'} \mathbf{S}_n^{H} \odot \mathbf{E}_1$. The combining vector for each substream is selected from the corresponding column in $\mathbf{V}_{lk}$. Nonetheless, it is not scalable due to its increasing complexity with the number of users. Inspired by [16], a scalable local PMMSE combiner for AP l is given with respect to its serving cluster as $\mathbf{V}_{lk} = \sqrt{\kappa_{\mathrm{t}} \kappa_{\mathrm{r}}} \left(\sum_{k' \in \mathcal{K}_l} \bar{\mathbf{\Psi}}_{lk} + \sigma^2 \mathbf{I}_M \right)^{-1} \hat{\mathbf{G}}_{lk} \mathbf{P}_{k}^{1/2}$. It is apparent that the computational complexity scales with the cardinal $|\mathcal{K}_l|$ which is usually constant and much smaller than the total

$$\mathrm{SINR}_{kn}^{\mathrm{MAX}} = \mathbb{E}\left\{\mathbf{b}_{knkn}^H\right\}\left(\sum_{k'=1}^{K}\sum_{n'=1}^{N}\frac{p_{k'}\xi_{k'n'}}{\kappa_{\mathrm{t}}}\mathbb{E}\left\{\mathbf{b}_{knk'n'}\mathbf{b}_{knk'n'}^H\right\} + \frac{1}{\kappa_{\mathrm{t}}\kappa_{\mathrm{r}}}\mathbf{F}_{kn} - \mathbb{E}\left\{\mathbf{b}_{knkn}\right\}\mathbb{E}\left\{\mathbf{b}_{knkn}^H\right\}\right)^{-1}\mathbb{E}\left\{\mathbf{b}_{knkn}\right\} \tag{9}$$

number of users in UC networks.

C. Hardware Distortion Correlation

The modeling assumptions of transceiver distortions can be derived via the Bussgang decomposition under two basic conditions:

- Both the input and output of the hardware are circularly symmetric complex Gaussian random variables.
- The power of the signal passing through the filter is maintained.

Referring to the results of element-wise distortions for MIMO systems in [53], we can decompose the output signal going through the non-linear filter $g(\cdot)$ as $\mathbf{y} = g(\mathbf{x}) = \mathbf{\Lambda}\mathbf{x} + \boldsymbol{\eta}$, where $\mathbf{x}$ and $\boldsymbol{\eta}$ represent the input signal and the additive distortion term, respectively. $\mathbf{\Lambda}$ is a diagonal matrix whose elements are composed of the Bussgang gains. Instead of fitting HIs with deterministic non-linear functions, we define $\mathbf{\Lambda}\mathbf{\Lambda}^H = \omega\mathbf{I}$ so that each antenna possesses the same hardware quality which is quantified by the factor ω. Thus, the additive distortion is distributed as $\mathcal{CN}(\mathbf{0}, (1-\omega)\mathbb{E}\{\mathbf{x}\mathbf{x}^H\})$. The hardware quality is directly proportional to ω ranging from 0 to 1, and $\omega = 1$ represents the ideal hardware without distortions. Note that the hardware quality factor can be calculated via any non-linearity with a concrete function.

Taking the UL data transmission as an example, we investigate the impact of the hardware distortion correlation as follows. Since we consider the UL transmission in this paper, the elements of the transmitter distortion $\boldsymbol{\eta}_{k,\mathrm{t}}$ are mutually uncorrelated owing to the independence between different data streams. If the receive distortions at different receive antennas are correlated, the conditional covariance of the correlated receive distortion is expressed as $\mathbf{C}_{l|\mathbf{G}}^{\mathrm{cor}} = (1-\kappa_{\mathrm{r}})\sum_{k=1}^{K}\mathbf{G}_k\mathbf{P}_k\mathbf{G}_k$. The unconditional distribution of the correlated distortion is expressed as $\boldsymbol{\eta}_{l,\mathrm{r}}^{\mathrm{cor}} = (1-\kappa_{\mathrm{r}})\sum_{k=1}^{K}\sum_{n=1}^{N}\sqrt{p_k\xi_{kn}}\bar{\eta}_{lkn}\mathbf{g}_{lkn}$, where $\bar{\eta}_{lkn}$ follows i.i.d. $\mathcal{CN}(0,1)$ for $\forall l, k, n$. Under this modeling assumption, the power of the correlated receiver distortion for substream n of user k with MRC is defined as

$$\begin{aligned}&\sum_{l=1}^{L}|a_{lkn}|^2\mathbb{E}\left\{\left|\hat{\mathbf{g}}_{lkn}^H\mathbf{D}_{lk}\boldsymbol{\eta}_{l,\mathrm{r}}\right|^2\right\}\\ =&(1-\kappa_{\mathrm{r}})\sum_{l\in\mathcal{L}_k}|a_{lkn}|^2\sum_{k'=1}^{K}\sum_{n'=1}^{N}p_{k'}\xi_{k'n'}\mathbb{E}\left\{\left|\hat{\mathbf{g}}_{lkn}^H\mathbf{g}_{lk'n'}\right|^2\right\},\end{aligned} \tag{11}$$

and the power of the uncorrelated receiver distortion for substream n of user k with MRC is defined as

$$\begin{aligned}&\sum_{l=1}^{L}|a_{lkn}|^2\mathbb{E}\left\{\left|\hat{\mathbf{g}}_{lkn}^H\mathbf{D}_{lk}\boldsymbol{\eta}_{l,\mathrm{r}}\right|^2\right\}\\ =&(1-\kappa_{\mathrm{r}})\sum_{l\in\mathcal{L}_k}|a_{lkn}|^2\sum_{k'=1}^{K}\sum_{n'=1}^{N}p_{k'}\xi_{k'n'}\mathbb{E}\left\{\|\hat{\mathbf{g}}_{lkn}\odot\mathbf{g}_{lk'n'}\|^2\right\}.\end{aligned} \tag{12}$$

Assuming perfect channel state information and independent spatial channels, we can get that $\mathbb{E}\{|\mathbf{g}_{lkn}^H\mathbf{g}_{lk'n'}|^2\} = \mathbb{E}\{\|\mathbf{g}_{lkn}\odot\mathbf{g}_{lk'n'}\|^2\} = M\beta_{lk}\beta_{lk'}$ for $k \neq k'$, and $\mathbb{E}\{|\mathbf{g}_{lkn}^H\mathbf{g}_{lk'n'}|^2\} = M(M+1)\beta_{lk}^2$ and $\mathbb{E}\{\|\mathbf{g}_{lkn}\odot\mathbf{g}_{lk'n'}\|^2\} = 2M\beta_{lk}^2$ for $k = k'$. The discrepancy occurs at $k = k'$, and the margin is $(M-1)M\beta_{lk}^2$ which is small when M is not very large. Although such uncorrelation makes the second condition dissatisfied, we can still get a tractable model for further derivations. In a CF mMIMO system, we would like to deploy more distributed APs instead of antennas employed at each AP [17]. Thus, it is reasonable that we assume the uncorrelations between different elements of receiver distortions, which have been successfully applied in [35], [37]–[39] to investigate the impact of HIs at the macro level. Note that we do not focus on any individual behavior of each hardware component in this paper, e.g., additive quantization noise, multiplicative phase drifts, amplified thermal noise, and so on.

D. Closed-form SE Expressions with MRC

Apparently, it is difficult to get the closed-form SE expression with the local MMSE combiner for the complicated shape of (10). For further research, an analytical expression is necessary. Referring to [17], we notice that channel hardening and favorable propagation can be primely obtained via multi-antenna APs. Thus, in the following theorem, we provide an exact and closed-form version of (7) with the low-complexity MRC scheme adopted at APs locally. Particularly, we utilize the LSFD method to strengthen the desired signal, restrain the inter-user and inter-stream interference, and enhance the achievable SE. The optimal LSFD coefficient vector and the maximized SE expression are also provided.

Theorem 2. *Using MRC that $\mathbf{v}_{lkn} = \hat{\mathbf{g}}_{lkn}$, the achievable UL SE of substream n for user k is expressed as (13) at the top of the next page. Corresponding vectors and matrices are expressed as*

$$\mathbf{b}_{kn} = [b_{kn,1}, \cdots, b_{kn,L}]^T, \tag{14}$$

$$\mathbf{\Upsilon}_{kn} = \mathrm{diag}(b_{kn,1}, \cdots, b_{kn,L}), \tag{15}$$

$$\mathbf{U}_{knk'n'} = \mathrm{diag}(u_{knk'n',1}, \cdots, u_{knk'n',L}), \tag{16}$$

$$\mathbf{Q}_{knk'n'} = \tau_p\kappa_{\mathrm{t}}\kappa_{\mathrm{r}}\mathbf{c}_{knk'n'}\mathbf{c}_{knk'n'}^H + \kappa_{\mathrm{r}}\mathbf{T}_{knk'n'} \tag{17}$$

$$\mathbf{\Lambda}_{knk'n'} = \mathrm{diag}(\lambda_{knk'n',1}, \cdots, \lambda_{knk'n',L}), \tag{18}$$

where $\mathbf{c}_{knk'n'} = [c_{knk'n',1}, \cdots, c_{knk'n',L}]^T$, $\mathbf{T}_{knk'n'} = \bar{\mathbf{T}}_{knk'n'}^H\mathbf{C}_{kk',1}\bar{\mathbf{T}}_{kn,k'n'}$, and the l-th column in $\bar{\mathbf{T}}_{knk'n'}$ is $\bar{\mathbf{t}}_{knk'n',l} = \mathrm{vec}(\mathbf{R}_{lk'}\mathbf{\Omega}_{lkn,n'}^H)$. Particularly, the elements defined above are expressed as $b_{kn,l} = \mathrm{tr}(\mathbf{D}_{lk}\mathbf{S}_n\hat{\mathbf{R}}_{lk}\mathbf{S}_n^H)$, $c_{knk'n',l} = \mathrm{tr}(\mathbf{\Xi}_{lknk'n'}\mathbf{R}_{lk'})$, and $u_{knk'n',l}$ and $\lambda_{knk'n',l}$ are given in (19) and (20) at the top of the next page, respectively.

Proof: Please refer to Appendix B, where the corresponding matrices are defined. ∎

Next, reconstructing the sum of elements with vector and matrix computations and using Corollary 2, we can get the optimal LSFD coefficient vector and the maximum achievable

$$\mathrm{SE}_{kn} = \left(1 - \frac{\tau_p}{\tau_c}\right) \log_2 \left(1 + \frac{p_k \xi_{kn} \left| \mathbf{a}_{kn}^H \mathbf{b}_{kn} \right|^2}{\mathbf{a}_{kn}^H \left(\sum_{k'=1}^{K} \sum_{n'=1}^{N} \frac{p_{k'} \xi_{k'n'}}{\kappa_\mathrm{t}} \left(\mathbf{U}_{knk'n'} + \mathbf{Q}_{knk'n'} + \frac{1-\kappa_\mathrm{r}}{\kappa_\mathrm{r}} \mathbf{\Lambda}_{knk'n'} \right) - p_k \xi_{kn} \mathbf{b}_{kn} \mathbf{b}_{kn}^H + \frac{\sigma^2}{\kappa_\mathrm{t}\kappa_\mathrm{r}} \mathbf{\Upsilon}_{kn} \right) \mathbf{a}_{kn}} \right) \tag{13}$$

$$\begin{aligned} u_{knk'n',l} = (1-\kappa_\mathrm{r}) \left\| \bar{\mathbf{\Omega}}_{lknk'n'} \mathbf{R}_{lk'} \mathbf{E}_2^H \odot \mathbf{I}_{MN} \right\|^2 + \sigma^2 \operatorname{tr} \left(\bar{\mathbf{\Omega}}_{lknn'} \mathbf{R}_{lk'} \bar{\mathbf{\Omega}}_{lknn'}^H \right) + \sum_{k''=1}^{K} \left(\tau_p \kappa_\mathrm{t} \kappa_\mathrm{r} \operatorname{tr} \left(\mathbf{\Xi}_{lknk''n'} \mathbf{R}_{lk'} \mathbf{\Xi}_{lknk''n'}^H \mathbf{R}_{lk''} \right) \right. \\ \left. + \kappa_\mathrm{r} \operatorname{tr} \left(\mathbf{C}_{kk'',1} \left(\left(\mathbf{\Omega}_{lknn'} \mathbf{R}_{lk'} \mathbf{\Omega}_{lknn'}^H \right)^T \otimes \mathbf{R}_{lk''} \right) \right) + (1-\kappa_\mathrm{r}) \operatorname{tr} \left(\bar{\mathbf{\Omega}}_{lknk''n''} \mathbf{R}_{lk'} \bar{\mathbf{\Omega}}_{lknk''n''}^H \odot \mathbf{E}_2 \mathbf{R}_{lk''} \mathbf{E}_2^H \right) \right) \end{aligned} \tag{19}$$

$$\begin{aligned} \lambda_{knk'n',l} =& \tau_p \kappa_\mathrm{t} \kappa_\mathrm{r} \left\| \mathbf{S}_{n'} \mathbf{R}_{lk'} \mathbf{\Xi}_{lknk'}^H \odot \mathbf{I}_M \right\|^2 + \kappa_\mathrm{r} \operatorname{vec} \left(\mathbf{S}_{n'} \mathbf{R}_{lk'} \right)^H \left(\mathbf{C}_{lknk',2} \odot \mathbf{E}_3 \right) \operatorname{vec} \left(\mathbf{S}_{n'} \mathbf{R}_{lk'} \right) \\ &+ (1-\kappa_\mathrm{r}) \left\| \bar{\mathbf{\Omega}}_{lkn,k'} \odot \mathbf{S}_{n'} \mathbf{R}_{lk'} \mathbf{E}_2^H \right\|^2 + \sigma^2 \operatorname{tr} \left(\bar{\mathbf{\Omega}}_{lkn} \bar{\mathbf{\Omega}}_{lkn}^H \odot \mathbf{S}_{n'} \mathbf{R}_{lk'} \mathbf{S}_{n'}^H \right) \\ &+ \sum_{k''=1}^{K} \left(\tau_p \kappa_\mathrm{t} \kappa_\mathrm{r} \operatorname{tr} \left(\mathbf{S}_{n'} \mathbf{R}_{lk'} \mathbf{S}_{n'}^H \odot \mathbf{\Xi}_{lknk''} \mathbf{R}_{lk''} \mathbf{\Xi}_{lknk''}^H \right) + \kappa_\mathrm{r} \operatorname{tr} \left(\left(\mathbf{R}_{lk''} \otimes \left(\mathbf{S}_{n'} \mathbf{R}_{lk'} \mathbf{S}_{n'}^H \odot \mathbf{I}_M \right) \right) \mathbf{C}_{lknk'',2}^T \right) \right. \\ &\left. + (1-\kappa_\mathrm{r}) \operatorname{tr} \left(\bar{\mathbf{\Omega}}_{lknk''} \left(\mathbf{E}_2 \mathbf{R}_{lk''} \mathbf{E}_2^H \odot \mathbf{I}_{MN\tau_p} \right) \bar{\mathbf{\Omega}}_{lknk''}^H \odot \mathbf{S}_{n'} \mathbf{R}_{lk'} \mathbf{S}_{n'}^H \right) \right) \end{aligned} \tag{20}$$

$$\mathbf{a}_{kn} = \left(\sum_{k'=1}^{K} \sum_{n'=1}^{N} p_{k'} \xi_{k'n'} \left(\kappa_\mathrm{r} \mathbf{U}_{knk'n'} + \kappa_\mathrm{r} \mathbf{Q}_{knk'n'} + (1-\kappa_\mathrm{r}) \mathbf{\Lambda}_{knk'n'} \right) + \sigma^2 \mathbf{\Upsilon}_{kn} \right)^{-1} \mathbf{b}_{kn} \tag{21}$$

$$\mathrm{SE}_{kn}^{\mathrm{MAX}} = \left(1 - \frac{\tau_p}{\tau_c}\right) \log_2 \left(1 + p_k \xi_{kn} \mathbf{b}_{kn}^H \left(\sum_{k'=1}^{K} \sum_{n'=1}^{N} \frac{p_{k'} \xi_{k'n'}}{\kappa_\mathrm{t}} \left(\mathbf{U}_{knk'n'} + \mathbf{Q}_{knk'n'} + \frac{1-\kappa_\mathrm{r}}{\kappa_\mathrm{r}} \mathbf{\Lambda}_{knk'n'} \right) - p_k \xi_{kn} \mathbf{b}_{kn} \mathbf{b}_{kn}^H + \frac{\sigma^2}{\kappa_\mathrm{t}\kappa_\mathrm{r}} \mathbf{\Upsilon}_{kn} \right)^{-1} \mathbf{b}_{kn} \right) \tag{22}$$

SE in closed form, which are given in (21) and (22) at the top of this page.

Remark 2. *We know that channels tend to harden as the number of antennas at APs increases, accompanied by favorable propagation. The spatial correlation could be neglected if $L \to \infty$. Hence, a similar conclusion can be drawn on hardware-quality scaling law in this system as Theorem 2 in [39] and Corollary 2 in [38] that augmenting the number of antennas or APs contributes to reducing demands on hardware quality. This agreement is also verified in the section on numerical results.*

IV. Uplink SE Analysis of MMSE-SIC detector

Unlike the linear decorrelator, the MMSE-SIC detector is an optimal receiver architecture for parallel data streams. However, it is hard to get the SINR of each data stream for the SIC during detection. In what follows, a lower bound is utilized to evaluate the achievable SE, which is derived via the mutual information between the input signal $\mathbf{s}_k$ and the second-layer combined signal $\tilde{\mathbf{s}}_k$. We extend the results in [31] to the hardware-impaired scenario and give the optimal LSFD coefficient matrix, which are also valid for arbitrary combining schemes. In addition, an approximate method is proposed herein to obtain the closed-form expression of the achievable SE for each user with MRC. We note that the existence of residual error brought by the SIC may deteriorate the SE while this is not the focus of this paper.

A. Generic SE Expressions

The transmission before the MMSE-SIC detector is the same as (1). Combined with $\mathbf{V}_{lk}$, the local estimate at AP l for user k is $\hat{\mathbf{s}}_{lk} = \mathbf{V}_{lk}^H \mathbf{y}_l$. Then, the CPU performs LSFD with large-scale fading coefficients as side information, and the signal combined at the CPU is expressed as

$$\begin{aligned} \tilde{\mathbf{s}}_k =& \sqrt{\kappa_\mathrm{r}} \sum_{l=1}^{L} \sum_{k'=1}^{K} \mathbf{A}_{lk}^H \mathbf{V}_{lk}^H \mathbf{D}_{lk} \mathbf{G}_{lk'} \left(\sqrt{\kappa_\mathrm{t}} \mathbf{P}_{k'}^{1/2} \mathbf{s}_{k'} + \boldsymbol{\eta}_{k',\mathrm{t}} \right) \\ &+ \sum_{l=1}^{L} \mathbf{A}_{lk}^H \mathbf{V}_{lk}^H \mathbf{D}_{lk} \boldsymbol{\eta}_{l,\mathrm{r}} + \sum_{l=1}^{L} \mathbf{A}_{lk}^H \mathbf{V}_{lk}^H \mathbf{D}_{lk} \mathbf{w}_l, \end{aligned} \tag{23}$$

where the LSFD coefficient matrix is denoted as $\mathbf{A}_k = [\mathbf{A}_{1k}^T, \cdots, \mathbf{A}_{Lk}^T]^T$. Note that $\mathbf{A}_k \in \mathbb{C}^{NL \times N}$ can also be optimized to maximize the lower bound of the achievable UL SE based on the MMSE scheme. Treating channel statistics as side information, the UatF bound is extended to the matrix version and calculated by virtue of the mutual information as the following corollary.

Corollary 3. *The achievable UL SE of user k with the MMSE-SIC detector is lower bounded by*

$$\mathrm{SE}_k^{\mathrm{LB}} = \left(1 - \frac{\tau_p}{\tau_c}\right) \log_2 \det \left(\mathbf{I}_N + \kappa_\mathrm{t} \kappa_\mathrm{r} \bar{\mathbf{G}}_k^H \bar{\mathbf{\Sigma}}_k^{-1} \bar{\mathbf{G}}_k \right), \tag{24}$$

where $\bar{\mathbf{G}}_k = \mathbf{A}_k^H \mathbb{E}\{\mathbf{Q}_{kk}\} \mathbf{P}_k^{1/2}$, $\bar{\mathbf{\Sigma}}_k = \mathbf{A}_k^H (\kappa_\mathrm{r} \sum_{k'=1}^{K} \mathbb{E}\{\mathbf{Q}_{kk'} \mathbf{P}_{k'} \mathbf{Q}_{kk'}^H\} + \mathbf{\Theta}_k) \mathbf{A}_k - \bar{\mathbf{G}}_k \bar{\mathbf{G}}_k^H$, *and we define that* $\mathbf{Q}_{kk'} = [(\mathbf{V}_{1k}^H \mathbf{D}_{1k} \mathbf{G}_{1k'})^T, \cdots, (\mathbf{V}_{Lk}^H \mathbf{D}_{Lk} \mathbf{G}_{Lk'})^T]^T$.

$$\mathrm{SE}_k^{\mathrm{MAX}} = \left(1-\frac{\tau_p}{\tau_c}\right)\log_2\det\left(\mathbf{I}_N + \kappa_{\mathrm{t}}\kappa_{\mathrm{r}}\mathbf{P}_k^{1/2}\mathbb{E}\left\{\mathbf{Q}_{kk}^H\right\}\left(\kappa_{\mathrm{r}}\sum_{k'=1}^{K}\mathbb{E}\left\{\mathbf{Q}_{kk'}\mathbf{P}_{k'}\mathbf{Q}_{kk'}^H\right\} + \mathbf{\Theta}_k - \kappa_{\mathrm{t}}\kappa_{\mathrm{r}}\mathbb{E}\left\{\mathbf{Q}_{kk}\right\}\mathbf{P}_k\mathbb{E}\left\{\mathbf{Q}_{kk}^H\right\}\right)^{-1}\mathbb{E}\left\{\mathbf{Q}_{kk}\right\}\mathbf{P}_k^{1/2}\right) \quad (25)$$

$$\mathrm{SE}_k^{\mathrm{LB}} \approx \left(1-\frac{\tau_p}{\tau_c}\right)\log_2\det\left(\mathbf{I}_N + \kappa_{\mathrm{t}}\kappa_{\mathrm{r}}\mathbf{A}_k^H\mathbf{Q}_k\mathbf{P}_k\mathbf{Q}_k^H\mathbf{A}_k\left(\mathbf{A}_k^H\left(\kappa_{\mathrm{r}}\sum_{k'=1}^{K}\bar{\mathbf{Q}}_{kk'}(1-\kappa_{\mathrm{r}})\mathbf{T}_k + \sigma^2\mathbf{S}_k - \kappa_{\mathrm{t}}\kappa_{\mathrm{r}}\mathbf{Q}_k\mathbf{P}_k\mathbf{Q}_k^H\right)\mathbf{A}_k\right)^{-1}\right) \quad (26)$$

Specifically, the l-th diagonal submatrix in $\mathbf{\Theta}_k = \mathrm{blkdiag}(\mathbf{\Theta}_{1k},\cdots,\mathbf{\Theta}_{Lk})$ is expressed as $\mathbf{\Theta}_{lk} = \sigma^2\mathbb{E}\{\mathbf{V}_{lk}^H\mathbf{D}_{lk}\mathbf{V}_{lk}\} + (1-\kappa_{\mathrm{r}})\mathbb{E}\{\mathbf{V}_{lk}^H(\sum_{k'=1}^{K}\mathbf{G}_{lk'}\mathbf{P}_{k'}\mathbf{G}_{lk'}^H \odot \mathbf{D}_{lk})\mathbf{V}_{lk}\}$.

Combined with the optimal LSFD coefficient matrix $\mathbf{A}_k = (\kappa_{\mathrm{r}}\sum_{k'=1}^{K}\mathbb{E}\{\mathbf{Q}_{kk'}\mathbf{P}_{k'}\mathbf{Q}_{kk'}^H\} + \mathbf{\Theta}_k)^{-1}\mathbb{E}\{\mathbf{Q}_{kk}\}\mathbf{P}_k^{1/2}$, the maximum achievable UL SE is given in (25) at the top of this page.

Proof: (24) and (25) can be derived following the similar procedures of Appendix A and C in [21], so the proof is omitted. The difference lies in that both the UC approach and HIs are further considered in this paper. ■

B. Closed-form SE Expressions with MRC

Next, instead of leaving the expectation operation in (24), we try to give a tractable version of the achievable UL SE. However, it is complicated to compute the exact expression of the second term in $\mathbf{\Theta}_{lk}$ due to the composite matrix computation. According to the definition of $\mathbf{D}_{lk}$, we observe that the correlation between $\mathbf{V}_{lk}$ and $\mathbf{G}_{lk'}$ in this term is weakened by the element-wise product with the diagonal matrix $\mathbf{D}_{lk}$ inside. Therefore, we can approximate the second term in $\mathbf{\Theta}_{lk}$ by assuming that $\mathbf{V}_{lk}$ is independent of $\mathbf{G}_{lk'}$ regardless of the value of index k and k'. In the end, we compute other expectations in (24) accurately to get the tight approximate expression as the following theorem.

Theorem 3. *Using MRC that $\mathbf{V}_{lk} = \hat{\mathbf{G}}_{lk}$, the closed-form achievable UL SE of user k is approximated as (26) at the top of this page, where*

$$\mathbf{Q}_k = \left[\mathbf{B}_{1k}^T,\cdots,\mathbf{B}_{Lk}^T\right]^T, \quad (27)$$

$$\mathbf{S}_k = \mathrm{blkdiag}\left\{\mathbf{B}_{1k},\cdots,\mathbf{B}_{Lk}\right\}, \quad (28)$$

$$\mathbf{T}_k = \mathrm{blkdiag}\left\{\mathbf{T}_{1k},\cdots,\mathbf{T}_{Lk}\right\}. \quad (29)$$

The (i,j)-th elements in the l-th submatrices of matrices above are expressed as $[\mathbf{B}_{lk}]_{ij} = \mathrm{tr}(\mathbf{S}_j\hat{\mathbf{R}}_{lk}\mathbf{S}_i)$ and $[\mathbf{T}_{lk}]_{ij} = \sum_{k'=1}^{K}\sum_{n'=1}^{N}\mathrm{tr}(\mathbf{S}_j\hat{\mathbf{R}}_{lk}\mathbf{S}_i \odot \mathbf{S}_{n'}\hat{\mathbf{R}}_{lk'}\mathbf{S}_{n'}^H)$. The (m,n)-th non-diagonal submatrix $\bar{\mathbf{Q}}_{kk',mn} \in \mathbb{C}^{N\times N}$ in $\bar{\mathbf{Q}}_{kk'} \in \mathbb{C}^{NL\times NL}$ is expressed as $\bar{\mathbf{Q}}_{kk',mn} = \mathbf{B}_{kk',m}\mathbf{P}_{k'}\mathbf{B}_{kk',n}^H$, where the (i,j)-th element in $\mathbf{B}_{kk',m}$ is expressed as $\left[\mathbf{B}_{kk',m}\right]_{ij} = \mathrm{tr}\left(\mathbf{S}_j\mathbf{R}_{mk'}\mathbf{\Xi}_{mkk'}\mathbf{S}_i^H\right)$ with $\mathbf{\Xi}_{mkk'} = \sqrt{\tau_{\mathrm{p}}\kappa_{\mathrm{t}}\kappa_{\mathrm{r}}}(\mathbf{P}_k^{1/2}\bar{\mathbf{\Phi}}_{k'k}^* \otimes \mathbf{I}_M)\mathbf{\Psi}_{mk}^H$. The submatrix on its diagonal is $\bar{\mathbf{Q}}_{kk',m} \in \mathbb{C}^{N\times N}$ for $m = 1,\cdots,L$, and its (i,j)-th element is expressed as $\left[\bar{\mathbf{Q}}_{kk',m}\right]_{ij} = p_{k'}\sum_{n=1}^{N}\xi_{k'n}q_{kk',n}^{mij}$, where $q_{kk',n}^{mij}$ is expressed as (30) at the top of the next page with

$$\mathbf{Z}_{kk'}^{mni} = \mathbf{S}_n^H\mathbf{S}_i\mathbf{\Psi}_{mk}\left(\bar{\mathbf{\Phi}}_{k'k}^T\mathbf{P}_k^{1/2}\otimes\mathbf{I}_M\right), \quad (31)$$

$$\mathbf{Y}_{kk'}^{mni} = \mathbf{S}_n^H\mathbf{S}_i\mathbf{\Psi}_{mk}\left(\mathbf{\Phi}_k^T\bar{\mathbf{P}}_{k'}^T\otimes\mathbf{I}_M\right). \quad (32)$$

Note that all submatrices are zero matrices when $\mathbf{D}_{lk} = \mathbf{0}^{M\times M}$.

Proof: See Appendix C. ■

Referring to the results in Theorem 3, we can also get the approximate maximized closed-form SE expression as (25) which is strengthened via the LSFD method. The expression is shown as (33) at the top of the next page. Since we only approximate the term of the receiver distortion in $\mathbf{\Theta}_{lk}$, the closed-form expression is exact in ideal hardware scenarios. If non-ideal hardware is employed, it would lose tightness for the loss of the partial correlation information in the receive distortion. Additionally, a suboptimal LSFD coefficient matrix can be given as

$$\mathbf{A}_k = \left(\kappa_{\mathrm{r}}\sum_{k'=1}^{K}\bar{\mathbf{Q}}_{kk'} + (1-\kappa_{\mathrm{r}})\mathbf{T}_k + \sigma^2\mathbf{S}_k\right)^{-1}\mathbf{Q}_k\mathbf{P}_k^{1/2}. \quad (34)$$

Note that (34) is an optimal LSFD coefficient matrix when the hardware is perfect.

Remark 3. *Different antennas may suffer from various degrees of non-linear distortions in reality. In this case, the concrete non-linear function should be considered instead of modeling the hardware quality with a constant factor [34]. We will discuss it in future research.*

V. Numerical Results and Discussions

In this section, Monte Carlo simulations are used to validate the theoretical results obtained above. We specifically explore the impact of HIs and different combining schemes. Apart from that, the scalability of the CF mMIMO system is discussed in the form of the UC approach and partial combining schemes.

A. Parameters Setup

Presuming that APs and users are uniformly distributed over a 0.5×0.5 km^2 square area, the large-scale fading coefficient β_{lk} is modeled as $\beta_{lk} = \mathrm{PL}_{lk}10^{\frac{\sigma_{\mathrm{sh}}z_{lk}}{10}}$, where PL_{lk} refers to the three-slope model [13] for the path loss and $z_{lk}\sim\mathcal{CN}(0,1)$. The receive spatial correlation matrix is modeled as (2.18) in [47]. We set $\tau_p = KN$, $D = 10$ cm, $\kappa_{\mathrm{t}} = 0.95$, and $\kappa_{\mathrm{r}} = 0.9$ unless mentioned, where D represents the size of the user. We consider a static network where $\mathcal{K}_l$ of AP l is predetermined by sorting large-scale fading coefficients. Other useful simulation parameters are listed in Table III.

$$
\begin{aligned}
q_{kk',n}^{mij} =& \tau_p \kappa_{\mathrm{t}} \kappa_{\mathrm{r}} \operatorname{tr}\left(\left(\mathbf{Z}_{kk'}^{mni}\right)^H \mathbf{R}_{mk'}\right) \operatorname{tr}\left(\mathbf{Z}_{kk'}^{mnj} \mathbf{R}_{mk'}\right) + \kappa_{\mathrm{r}} \operatorname{vec}\left(\left(\mathbf{Z}_{k}^{mnj}\right)^H \mathbf{R}_{mk'}\right) \mathbf{C}_{kk'',1} \operatorname{vec}\left(\left(\mathbf{Z}_{k}^{mni}\right)^H \mathbf{R}_{mk'}\right) \\
&+ (1-\kappa_{\mathrm{r}}) \operatorname{tr}\left(\left(\mathbf{Y}_{kk'}^{mni}\right)^H \mathbf{R}_{mk'} \mathbf{E}_2^H \odot \mathbf{E}_2 \mathbf{R}_{mk'} \mathbf{Y}_{kk'}^{mnj}\right) + \sigma^2 \operatorname{tr}\left(\left(\mathbf{Z}_{k}^{mni}\right)^H \mathbf{R}_{mk'} \mathbf{Z}_{k}^{mnj} \left(\bar{\mathbf{\Phi}}_{kk}^{*} \otimes \mathbf{I}_M\right)\right) \\
&+ \sum_{k''=1}^{K} \left(\tau_p \kappa_{\mathrm{t}} \kappa_{\mathrm{r}} \operatorname{tr}\left(\left(\mathbf{Z}_{kk''}^{mni}\right)^H \mathbf{R}_{mk'} \mathbf{Z}_{kk''}^{mnj} \mathbf{R}_{mk''}\right) + \kappa_{\mathrm{r}} \operatorname{tr}\left(\mathbf{C}_{kk'',1} \left(\mathbf{R}_{mk''}^{T} \otimes \left(\mathbf{Z}_{k}^{mni}\right)^H \mathbf{R}_{mk'} \mathbf{Z}_{k}^{mnj}\right)\right) \right. \\
&\left. + (1-\kappa_{\mathrm{r}}) \operatorname{tr}((\mathbf{Y}_{kk''}^{mni})^H \mathbf{R}_{mk'} \mathbf{Y}_{kk''}^{mnj} \odot \mathbf{E}_2 \mathbf{R}_{mk''} \mathbf{E}_2^H) \right)
\end{aligned} \tag{30}
$$

$$
\mathrm{SE}_k^{\mathrm{MAX}} \approx \left(1 - \frac{\tau_p}{\tau_c}\right) \log_2 \det\left(\mathbf{I}_{NL} + \kappa_{\mathrm{t}} \kappa_{\mathrm{r}} \mathbf{Q}_k \mathbf{P}_k \mathbf{Q}_k^H \left(\kappa_{\mathrm{r}} \sum_{k'=1}^{K} \bar{\mathbf{Q}}_{kk'} + (1-\kappa_{\mathrm{r}}) \mathbf{T}_k + \sigma^2 \mathbf{S}_k - \kappa_{\mathrm{t}} \kappa_{\mathrm{r}} \mathbf{Q}_k \mathbf{P}_k \mathbf{Q}_k^H \right)^{-1} \right) \tag{33}
$$

TABLE III
PARAMETERS FOR THE SIMULATION

Parameter	Value
Noise power σ^2	$-203.975 + 10\lg(B) + F$ dBW
Bandwidth B	20 MHz
Noise figure F	9 dB
Standard deviation of shadow fading σ_{sh}	8 dB
Angular standard deviation of azimuth angle σ_ψ and elevation angle σ_θ	15°
Length of coherence block τ_c	200
Transmit power p_k	200 mW
Power control factor ξ_{kn}	$1/N$
Cardinality of UC service cluster $\lvert\mathcal{K}_l\rvert$	K_{S}

B. Performance Evaluation

In Fig. 2, we show the cumulative distribution function (CDF) of the per-user SE with MRC and compare the linear decorrelator with the MMSE-SIC detector. Fig. 2 simulates the scenario with $L = 20$, $M = 4$, $K = 5$, and $N = 4$, where the antenna spacing d_k is computed as $D/(N-1)$. Besides, in the UC case, we let $K_{\mathrm{S}} = 2$. The analytical results coincide with the simulations in different situations, confirming the precision of the closed-form SE expressions of (22) and (33). We observe that 95%-likely per-user SE with the MMSE-SIC detector is about 0.5 bits/s/Hz higher than that with the linear decorrelator under perfect hardware quality in the CF case. The MMSE-SIC detector outperforms the linear decorrelator due to the SIC which facilitates suppressing the interference from multiple data streams. However, the residual analysis in the SIC is dismissed for over complexity, and the existence of the residual may bring about extra interference. For 50%-likely per-user SE, the performance loss of the MMSE-SIC detector is about 24% in the UC case with HIs compared to that in the CF case with perfect hardware while its counterpart of the linear decorrelator is about 19%. It means that the degradation of SE with the MMSE-SIC detector is more rapid than that with the linear decorrelator.

We investigate the effect of the hardware-quality scaling law in Fig. 3, where curves of the sum SE are plotted with different scaling exponents against the number of APs. We define the hardware quality factors as $\kappa_{\mathrm{t}} = \frac{\bar{\kappa}_{\mathrm{t}}}{L^{\varepsilon_{\mathrm{t}}}}$ and $\kappa_{\mathrm{r}} = \frac{\bar{\kappa}_{\mathrm{r}}}{L^{\varepsilon_{\mathrm{r}}}}$, where ε_{t} and ε_{r} denote scaling exponents. The other setups are identical to that in Fig. 2. Referring to Remark 2, we set $\varepsilon_{\mathrm{t}} = 0$, $\varepsilon_{\mathrm{r}} \in \{0, 1/16, 1/3, 1/2, 2/3\}$, and $\bar{\kappa}_{\mathrm{t}} = \bar{\kappa}_{\mathrm{r}} = 0.997$. Fig. 3 shows that the SE loss resulting from low-cost hardware can be offset by increasing the number of APs and receive antennas when $\varepsilon_{\mathrm{t}} = 0$ and $\varepsilon_{\mathrm{r}} \in (0, 1/2)$. We can conclude that the smaller scaling exponent contributes to the smaller SE loss, but if $\varepsilon_{\mathrm{r}} > 1/2$, the hardware-quality scaling law would fail. Whereas, increasing the number of APs or receive antennas may apparently lead to higher costs, which is contradictory to the original intention for scalability. Energy and economic efficiency are two effective metrics to find a tradeoff between the number of APs and performance under HIs, and we leave it for future research. Moreover, we recommend the radio stripe as an alternative to the traditional AP, whose costs are considerably low [12].

Fig. 4 compares the per-user SE under different designs of $\mathbf{a}_{kn}$ with the MMSE combiner and MRC. In Fig.4(a), we observe that there is a marked increase in the per-user SE by using the optimal LSFD with MRC. Comparing S-CD

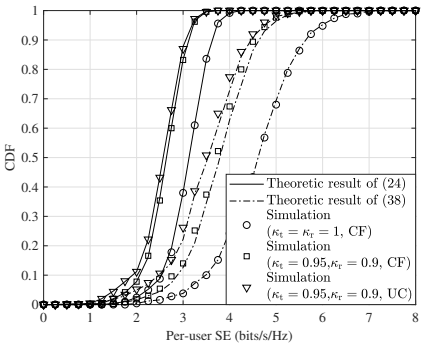

Fig. 2. CDF of per-user SE with MRC for linear decorrelators and MMSE-SIC detectors.

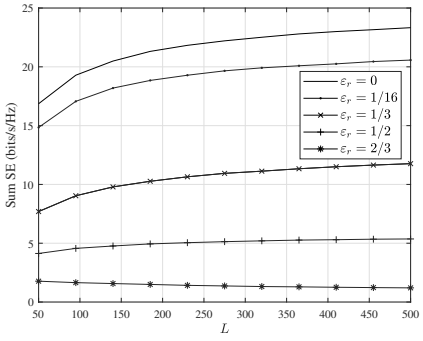

Fig. 3. Sum SE against the number of APs for the hardware-quality scaling law with different exponents.

This article has been accepted for publication in a future issue of this journal, but has not been fully edited. Content may change prior to final publication. Citation information: DOI10.1109/TBC..., IEEE Transactions on Wireless Communications

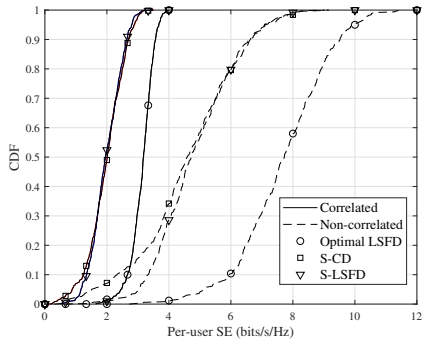

(a) MRC

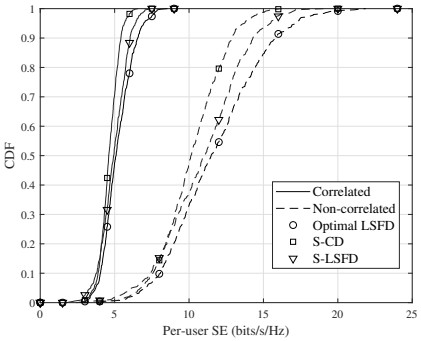

(b) MMSE combining

Fig. 4. CDF of per-user SE with different LSFD coefficients over correlated and uncorrelated channels.

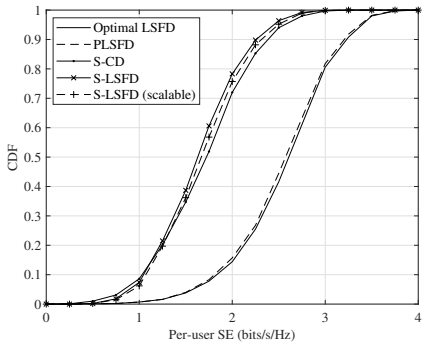

(a) Linear decorrelator

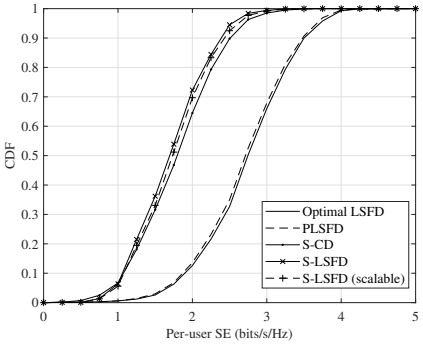

(b) MMSE-SIC detector

Fig. 5. CDF of per-user SE with MRC and different LSFD coefficients for linear decorrelators and MMSE-SIC detectors.

to S-LSFD, the 95%-likely users can benefit from S-LSFD, especially over uncorrelated channels. Further, in Fig.4(b), we can see that the performance gap between the optimal LSFD and S-LSFD with MMSE is much smaller than that with MRC, and 95%-likely users can reach near performance under different LSFD coefficients. Interestingly, the privilege of optimal LSFD and S-LSFD only appears in the users with higher SE when utilizing the MMSE combiner, which is the opposite of MRC.

Next, we consider a high dense CF network with $L = 50$, $K = 10$, $M = N = 2$, $K_S = 2$, and antenna spacing $d_k = 5$ cm in Fig. 5. From Fig. 5(a), it can be seen that the SE of PLSFD is slightly lower than LSFD, while the SE of scalable S-LSFD is slightly higher than S-LSFD. The same phenomenon appears at the MMSE-SIC detector as shown in Fig. 5(b). These results demonstrate that the LSFD coefficients are mainly influenced by several closest users for each AP. Thus, scalable LSFD contributes to reducing computational complexity and maintaining communication quality at the same time. Moreover, we find that S-CD can achieve better performance in the high-dense network compared to S-LSFD. Since the linear decorrelator and the MMSE-SIC detector have a similar variation trend, we only simulate the results of the linear decorrelator to investigate the hardware distortion correlation, the UC approach, and the optimal number of transmit antennas.

In Fig. 6, we investigate the impact of the hardware distortion correlation on the linear decorrelator with $L = 20$, $K = 5$, and $N = 4$. It corresponds to the analyses before that the hardware distortion correlation declines the SE but is negligible when M is small and κ_r is close to 1. Additionally, the optimal LSFD contributes to weakening the impact of the hardware distortion correlation due to its ability to suppress interference.

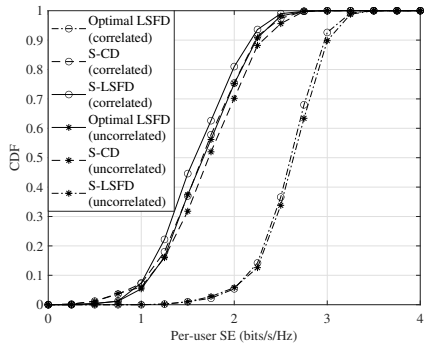

(a) $M = 4$ and $\kappa_r = 0.9$

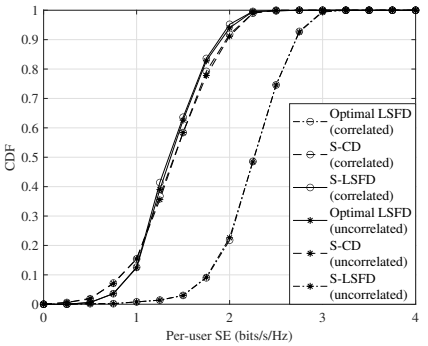

(b) $M = 2$ and $\kappa_r = 0.95$

Fig. 6. CDF of per-user SE with MRC under correlated and uncorrelated hardware distortions.

This article has been accepted for publication in a future issue of this journal, but has not been fully edited. Content may change prior to final publication. Citation information: DOI10.1109/TBC..., IEEE Transactions on Wireless Communications

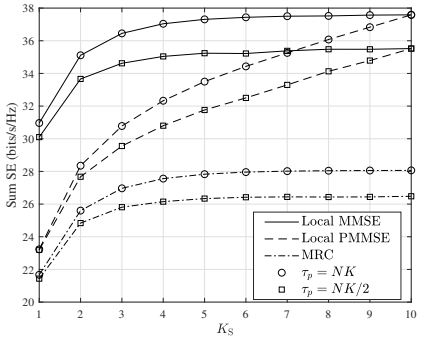

Fig. 7. Average sum SE against the size of UC clusters K_S with different combining schemes.

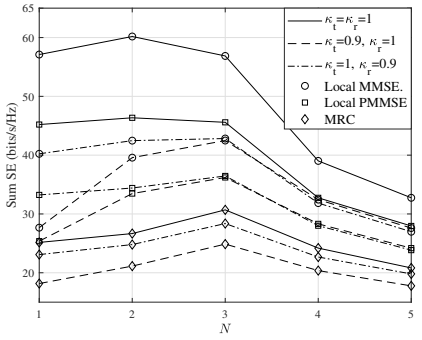

Fig. 8. Average sum SE against the number of transmit antennas N for different combining schemes and HIs.

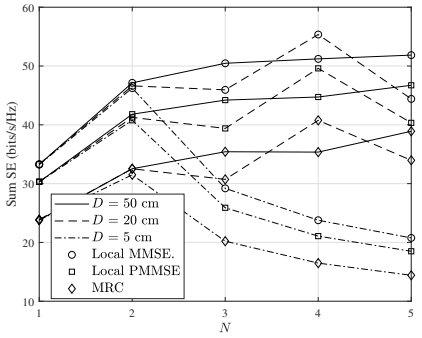

Fig. 9. Average sum SE against the number of transmit antennas N for different combining schemes and D.

Instead of estimating the signal from all users in the CF case, the UC approach is a scalable way to reduce the computational complexity that only users in the cluster $\mathcal{K}_l$ are combined and transferred to the CPU by AP l. In Fig. 7, we show the average sum SE with different combining schemes over different τ_p against the size of serving cluster K_S in the same high-dense scenario as in Fig. 5. We observe that the SE of PMMSE is higher than MRC while lower than MMSE, and it increases with the K_S. This makes the PMMSE combiner a scalable and low-complexity substitution of the MMSE combiner. The performance loss is quite trivial for $K_S = 7$ compared to $K_S = 10$ which denotes the CF case. Even when $K_S = 5$, the performance loss is still acceptable. This result inspires us that each AP only needs to serve half of the users with the local MMSE combiner and MRC even if HIs and pilot contaminations both exist.

Finally, we consider another UC CF network with $L = 40$, $K = 10$, $M = 4$, and $K_S = 5$. In Fig. 8, we show the average sum SE as a function of the number of transmit antennas with the local MMSE and PMMSE combiners and MRC for different hardware quality factors. When $\kappa_t = \kappa_r = 1$, the optimal number of transmit antennas is 2 for the local MMSE and PMMSE combiners, and it rises to 3 when HIs exist. Whereas, the optimal number for MRC remains 3 steady as the hardware quality changes. It reveals that the higher SE cannot be achieved with the indefinitely growing number of transmit antennas. What else can be seen is that HIs at transmitters bring more decrease in performance compared to those at receivers.

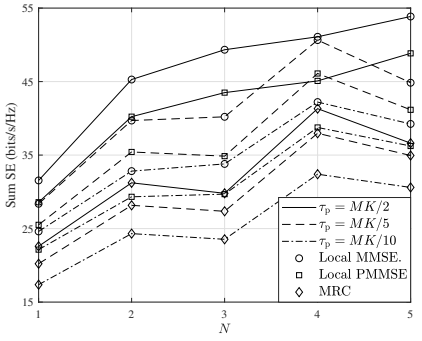

Fig. 10. Average sum SE against the number of transmit antennas N for different combining schemes and τ_p.

In Fig. 9, we show the effect of three different sizes of users with different combining schemes, where we set $\kappa_t = 0.95$ and $\kappa_r = 0.9$. With the size of users getting larger, the CF UC network can support users with more transmit antennas. When $D = 50$ cm, the optimal N is larger than 5 for both the MRC, and the local MMSE and PMMSE combiner. As D decreases to 20 cm and 5 cm, the optimal N shrinks to 4 and 2, respectively.

In Fig. 10, we continue to investigate the effect of three different lengths of the pilot sequence τ_p with different combining schemes. When $\tau_p = NK/2$, the optimal N is larger than 5 for all three combining schemes. As τ_p decreases to $NK/5$ and $NK/10$, the optimal N shrinks to 4. It indicates that the optimal N would be decreased with high pilot contaminations. Moreover, all three figures above confirm that an optimal number of transmit antennas should be obtained.

VI. CONCLUSION

This paper studied the achievable UL SE of a hardware-impaired UC CF mMIMO system with both multi-antenna APs and multi-antenna users over joint-correlated Rayleigh fading channels. We derived the closed-form achievable UL SE expressions with MRC for both the linear decorrelator and the MMSE-SIC detector. The hardware quality scaling law was shown to be applicable with multi-antenna users that HIs at APs can be controllable by increasing the number of receive antennas. Moreover, compared to the S-LSFD, the S-CD is a better choice in the spatial-correlated and hardware-impaired system when the optimal LSFD is not available. Besides, in the UC CF network, each AP only needs to serve half of the neighboring users to reach near SE compared to the CF mMIMO with the local MMSE combiner and MRC. Note that the local PMMSE combiner can be a scalable alternative that

outperforms MRC and has lower complexity than the local MMSE combiner.

In the future, we will investigate other enhance combining/precoding schemes, such as the enhanced normalized conjugate beamforming and local partial zero-forcing for both the UL and DL CF mMIMO systems with multi-antenna users over Rician fading channels. Furthermore, we will study limited fronthaul links, especially wireless fronthaul links.

Appendix A
Useful Lemmas

This appendix contains several lemmas associated with calculations of the random matrix, where we aim at rewriting the sums of elements using matrix computations and eliminating the expectations. At first, we define a few assisted vectors and matrices that $\mathbf{a}$, $\mathbf{b}$, $\mathbf{A}$, and $\mathbf{B}$ are any complex deterministic vectors and matrices. Second, we define some random vectors and matrices $\mathbf{x} \sim \mathcal{CN}(\mathbf{0}, \mathbf{R}_x)$, $\mathbf{y} \sim \mathcal{CN}(\mathbf{0}, \mathbf{R}_y)$, and $\mathbf{Z} \sim \mathcal{CN}(\mathbf{0}, \mathbf{R}_z)$. Specifically, multiple summation notations with respect to different subscripts are replaced with a single $\sum$ as a brief representation here, and the number of sum symbols is marked on the top. It holds that

Lemma 1. For $\mathbf{x}, \mathbf{y} \in \mathbb{C}^{M\times 1}$, $\mathbf{Z} \in \mathbb{C}^{M\times N}$, and $\mathbf{A}, \mathbf{B} \in \mathbb{C}^{N\times M}$,

$$\mathbb{E}\{\mathbf{x}^H\mathbf{Z}\mathbf{A}\mathbf{x}\mathbf{y}^H\mathbf{B}^H\mathbf{Z}^H\mathbf{y}\} = \mathrm{vec}(\mathbf{R}_x\mathbf{A}^H)^H\mathbf{R}_z\,\mathrm{vec}(\mathbf{R}_y\mathbf{B}^H). \quad (35)$$

Proof: Utilizing the independence between $\mathbf{x}$, $\mathbf{y}$ and $\mathbf{Z}$, it follows that

$$\begin{aligned}&\mathbb{E}\{\mathbf{x}^H\mathbf{Z}\mathbf{A}\mathbf{x}\mathbf{y}^H\mathbf{B}^H\mathbf{Z}^H\mathbf{y}\}\\ &=\sum^{8} a_{n_1m_1'}b^*_{n_2m_2'}\mathbb{E}\left\{z_{m_1n_1}z^*_{m_2n_2}x^*_{m_1'}x_{m_1'}y_{m_2}y^*_{m_2'}\right\}\\ &=\sum^{6} a_{n_1m_1'}b^*_{n_2m_2'}r_{z,m_1n_1m_2n_2}r^*_{x,m_1m_1'}r_{y,m_2m_2'},\end{aligned} \quad (36)$$

where $r_{z,m_1n_1m_2n_2}$ is the $((n_1-1)M+m_1,(n_2-1)M+m_2)$-th element of $\mathbf{R}_z$. Combining the elements with subscript m_1', we can get $\sum^1 a_{n_1m_1'}r^*_{x,m_1m_1'} = [\mathbf{R}_x\mathbf{A}^H]^*_{m_1n_1}$. Similarly, we have $\sum^1 b^*_{n_2m_2'}r_{y,m_2m_2'} = [\mathbf{R}_y\mathbf{B}^H]_{m_2n_2}$, and we can reconstruct (36) as the matrix form of (35). ∎

Lemma 2. For $\mathbf{x} \in \mathbb{C}^{M\times 1}$, $\mathbf{y} \in \mathbb{C}^{P\times 1}$, $\mathbf{Z} \in \mathbb{C}^{M\times N}$, and $\mathbf{A} \in \mathbb{C}^{N\times P}$,

$$\mathbb{E}\{|\mathbf{x}^H\mathbf{Z}\mathbf{A}\mathbf{y}|^2\} = \mathrm{tr}(\mathbf{R}_z((\mathbf{A}\mathbf{R}_y\mathbf{A}^H)^T\otimes\mathbf{R}_x)). \quad (37)$$

Proof: We first eliminate the randomness of $\mathbf{y}$ as $\mathbb{E}\{|\mathbf{x}^H\mathbf{Z}\mathbf{A}\mathbf{y}|^2\} = \mathbb{E}\{\mathbf{x}^H\mathbf{Z}\mathbf{C}\mathbf{Z}^H\mathbf{x}\}$, where $\mathbf{C} = \mathbf{A}\mathbf{R}_y\mathbf{A}^H$. Then, we have

$$\begin{aligned}\mathbb{E}\{\mathbf{x}^H\mathbf{Z}\mathbf{C}\mathbf{Z}^H\mathbf{x}\} &\overset{(a)}{=} \sum^{4} c_{nn'}r_{z,mnm'n'}r_{x,m'm}\\ &= \mathrm{sum}(\mathbf{R}_z\odot(\mathbf{C}\otimes\mathbf{R}_x^T)),\end{aligned} \quad (38)$$

where (a) is obtained via (36) and $\mathrm{sum}(\mathbf{A})$ denotes the sum of all the elements in matrix $\mathbf{A}$. Through (1.9.6) in [56], (38) can be simplified as (37). ∎

Lemma 3. For $\mathbf{x} \in \mathbb{C}^{M\times 1}$, $\mathbf{Z} \in \mathbb{C}^{M\times N}$, and $\mathbf{A} \in \mathbb{C}^{N\times M}$,

$$\begin{aligned}\mathbb{E}\{|\mathbf{x}^H\mathbf{Z}\mathbf{A}\mathbf{x}|^2\} =& \,\mathrm{vec}(\mathbf{R}_x\mathbf{A}^H)^H\mathbf{R}_z\,\mathrm{vec}(\mathbf{R}_x\mathbf{A}^H)\\ &+\mathrm{tr}(\mathbf{R}_z((\mathbf{A}\mathbf{R}_x\mathbf{A}^H)^T\otimes\mathbf{R}_x)).\end{aligned} \quad (39)$$

Proof: Note that $\mathbf{x}$ is equivalent to $\mathbf{S}_x\bar{\mathbf{x}}$ with $\mathbf{S}_x = \mathbf{R}_x^{1/2}$ and $\bar{\mathbf{x}} \sim \mathcal{CN}(\mathbf{0}, \mathbf{I}_M)$, and we define $\mathbf{C}_x = \mathbf{A}\mathbf{S}_x$. Hence, we can rewrite $\mathbb{E}\{|\mathbf{x}^H\mathbf{Z}\mathbf{A}\mathbf{x}|^2\}$ as $\mathbb{E}\{|\bar{\mathbf{x}}^H\mathbf{S}_x^H\mathbf{Z}\mathbf{C}_x\bar{\mathbf{x}}|^2\}$ and expand it as

$$\begin{aligned}\mathbb{E}\{|\bar{\mathbf{x}}^H\mathbf{S}_x^H\mathbf{Z}\mathbf{C}_x\bar{\mathbf{x}}|^2\} &= \mathbb{E}\{|\sum^{4}\bar{x}^*_{m_1}s^*_{x,mm_1}z_{mn}c_{x,nm_2}\bar{x}_{m_2}|^2\}\\ &\overset{(a)}{=} \sum^{6} s^*_{x,mm_1}s_{x,m'm_1'}c_{x,nm_1}c^*_{x,n'm_1'}r_{z,mnm'n'}\\ &\quad+\sum^{6} s^*_{x,mm_1}s_{x,m'm_1}c_{x,nm_2}c^*_{x,n'm_2}r_{z,mnm'n'}\\ &\overset{(b)}{=} \mathrm{vec}\left(\mathbf{S}_x\mathbf{C}_x^H\right)^H\mathbf{R}_z\mathrm{vec}\left(\mathbf{S}_x\mathbf{C}_x^H\right)+\mathrm{sum}\left(\mathbf{R}_z\odot\left(\mathbf{C}_x\mathbf{C}_x^H\otimes\mathbf{R}_x^T\right)\right),\end{aligned} \quad (40)$$

where (a) utilizes that $\mathbb{E}\{\bar{x}^*_{m_1}\bar{x}_{m_1'}\bar{x}_{m_2}\bar{x}^*_{m_2'}\}$ is non-zero only when $m_1 = m_1' = m_2 = m_2'$, $m_1 = m_1'$ and $m_2 = m_2'$ with $m_1 \neq m_2$, and $m_1 = m_2$ and $m_1' = m_2'$ with $m_1 \neq m_1'$. In (b), we exploit that $\sum^1 s^*_{x,mm_1}c_{x,nm_1} = [\mathbf{S}_x\mathbf{C}_x^H]^*_{mn}$, $\sum s_{x,m'm_1'}c^*_{x,n'm_1'} = [\mathbf{S}_x\mathbf{C}_x^H]_{m'n'}$, $\sum^1 s^*_{x,mm_1}s_{x,m'm_1} = r^*_{x,mm'}$, and $\sum^1 c_{x,nm_2}c^*_{x,n'm_2} = [\mathbf{C}_x\mathbf{C}_x^H]_{nn'}$ with the derivations in Lemma 1 and 2. ∎

Lemma 4. For $\mathbf{x} \in \mathbb{C}^{N\times 1}$, $\mathbf{y} \in \mathbb{C}^{P\times 1}$, $\mathbf{A} \in \mathbb{C}^{M\times P}$, and $\mathbf{Z} \in \mathbb{C}^{M\times N}$,

$$\mathbb{E}\left\{\|\mathbf{Z}\mathbf{x}\odot\mathbf{A}\mathbf{y}\|^2\right\} = \mathrm{tr}\left(\left(\mathbf{R}_x\otimes\left(\mathbf{A}\mathbf{R}_y\mathbf{A}^H\odot\mathbf{I}_M\right)\right)\mathbf{R}_z^T\right). \quad (41)$$

Proof: We expand that

$$\begin{aligned}\mathbb{E}\left\{\|\mathbf{Z}\mathbf{x}\odot\mathbf{A}\mathbf{y}\|^2\right\} &= \sum^{1}\mathbb{E}\{|\sum^{2} z_{mn}x_na_{mp}y_p|^2\}\\ &\overset{(a)}{=} \sum^{3} r_{z,mnm'n'}[\mathbf{A}\mathbf{R}_y\mathbf{A}^H]_{mm}r_{x,nn'}\\ &= \mathrm{sum}\left(\mathbf{R}_z\odot\left(\mathbf{R}_x\otimes\left(\mathbf{A}\mathbf{R}_y\mathbf{A}^H\odot\mathbf{I}_M\right)\right)\right),\end{aligned} \quad (42)$$

where (a) utilizes that $\sum^2 a_{mp}r_{y,pp'}a^*_{mp'} = [\mathbf{A}\mathbf{R}_y\mathbf{A}^H]_{mm}$. We need to mention that (a) only hinges on the diagonal elements of $\mathbf{A}\mathbf{R}_y\mathbf{A}^H$. Therefore, we can reconstruct (42) via (38). ∎

Lemma 5. For $\mathbf{x} \in \mathbb{C}^{N\times 1}$ and $\mathbf{A}, \mathbf{Z} \in \mathbb{C}^{M\times N}$,

$$\begin{aligned}\mathbb{E}\{\|\mathbf{Z}\mathbf{x}\odot\mathbf{A}\mathbf{x}\|^2\} =& \,\mathrm{tr}((\mathbf{R}_x\otimes(\mathbf{A}\mathbf{R}_x\mathbf{A}^H\odot\mathbf{I}_M))\mathbf{R}_z^T)\\ &+\mathrm{vec}(\mathbf{A}_x\mathbf{R}_x)^H(\mathbf{R}_z\odot\mathbf{E}_4)\,\mathrm{vec}(\mathbf{A}_x\mathbf{R}_x),\end{aligned} \quad (43)$$

where the constant matrix $\mathbf{E}_4 = \mathbf{1}^{N\times N}\otimes\mathbf{I}_M$.

Proof: Similar to the proof of Lemma 3, we can write

$$\begin{aligned}\mathbb{E}\left\{\|\mathbf{Z}\mathbf{x}\odot\mathbf{A}\mathbf{x}\|^2\right\} &= \mathbb{E}\left\{\|\mathbf{Z}\mathbf{S}_x\bar{\mathbf{x}}\odot\mathbf{C}_x\bar{\mathbf{x}}\|^2\right\}\\ &= \sum^{1}\mathbb{E}\{|\sum^{3} z_{mn}s_{x,nn_1}\bar{x}_{n_1}c_{x,mn_2}\bar{x}_{n_2}|^2\}\\ &\overset{(a)}{=} \sum^{5} s_{x,nn_1}s^*_{x,n'n_1}c_{x,mn_2}c^*_{x,mn_2}r_{z,mnmn'}\\ &\quad+\sum^{5} s_{x,nn_1}s^*_{x,n'n_2}c_{x,mn_2}c^*_{x,mn_1}r_{z,mnmn'}.\end{aligned} \quad (44)$$

where we define $\mathbf{C}_x = \mathbf{A}\mathbf{S}_x$. In (a), we can compute that $r_{x,nn'} = \sum^1 s_{x,nn_1}s^*_{x,n'n_1}$, $[\mathbf{C}_x\mathbf{C}_x^H]_{mm} = \sum^1 c_{x,mn_2}c^*_{x,mn_2}$, $[\mathbf{C}_x\mathbf{S}_x]^*_{mn} = \sum^1 c^*_{x,mn_1}s^*_{x,n_1n}$, and $[\mathbf{C}_x\mathbf{S}_x]_{mn'} = \sum^1 c_{x,mn_2}s_{x,n_2n'}$, respectively. Then, via the result of (42), we can rewrite the first term as $\mathrm{tr}\left(\left(\mathbf{R}_x\otimes\left(\mathbf{C}_x\mathbf{C}_x^H\odot\mathbf{I}_M\right)\right)\mathbf{R}_z^T\right)$,

$$\mathrm{B}^{(1)}_{knk'n'k''} = \sum_{l=1}^{L} |a_{lkn}|^2 \operatorname{tr}\left(\boldsymbol{\Xi}_{lknk''n'}\mathbf{R}_{lk'}\boldsymbol{\Xi}^H_{lknk''n'}\mathbf{R}_{lk''}\right) + \begin{cases} 0 & , k'' \neq k' \\ \left|\sum\limits_{l=1}^{L} a^*_{lkn} \operatorname{tr}\left(\boldsymbol{\Xi}_{lknk'n'}\mathbf{R}_{lk'}\right)\right|^2 & , k'' = k' \end{cases} \tag{50}$$

$$\mathrm{B}^{(2)}_{knk'n'k''} = \sum_{l=1}^{L} |a_{lkn}|^2 \operatorname{tr}\left(\mathbf{C}_{kk'',1}\left(\left(\boldsymbol{\Omega}_{lknn'}\mathbf{R}_{lk'}\boldsymbol{\Omega}^H_{lknn'}\right)^T \otimes \mathbf{R}_{lk'}\right)\right) + \begin{cases} 0 & , k'' \neq k' \\ \left(\sum\limits_{l=1}^{L} a^*_{lkn}\bar{\mathbf{t}}^H_{knk'n',l}\right)\mathbf{C}_{kk',1}\left(\sum\limits_{l=1}^{L} a_{lkn}\bar{\mathbf{t}}_{knk'n',l}\right) & , k'' = k' \end{cases} \tag{51}$$

and the second term is rewritten via the result of (35) as $\operatorname{vec}(\mathbf{C}_x\mathbf{S}_x)^H(\mathbf{R}_z \odot \mathbf{E}_4)\operatorname{vec}(\mathbf{C}_x\mathbf{S}_x)$. ■

Appendix B
Proof of Theorem 2

The main work is to derive A_{lkn}, $\mathrm{B}_{lkn,k'n'}$, $\mathrm{C}_{lkn,k'n'}$, and D_{lkn} in Corollary 1 with $\mathbf{v}_{lkn} = \hat{\mathbf{g}}_{lkn}$. Starting with A_{lkn} and D_{lkn}, we can easily get that $b_{kn,l} = \mathbb{E}\{\mathbf{v}^H_{lkn}\mathbf{D}_{lk}\mathbf{g}_{lkn}\} = \operatorname{tr}(\mathbf{D}_{lk}\mathbf{S}_n\hat{\mathbf{R}}_{lk}\mathbf{S}^H_n)$. Thereafter, we decompose $\mathrm{B}_{knk'n'}$ via channel estimates in (4) as

$$\begin{aligned}\mathrm{B}_{knk'n'} =& \tau_p\kappa_{\mathrm{t}}\kappa_{\mathrm{r}}\sum_{k''=1}^{K}\mathrm{B}^{(1)}_{knk'n'k''} + \kappa_{\mathrm{r}}\sum_{k''=1}^{K}\mathrm{B}^{(2)}_{knk'n'k''} \\ &+ \sum_{l=1}^{L}|a_{lkn}|^2\,\mathrm{B}^{(3)}_{lknk'n'} + \sum_{l=1}^{L}|a_{lkn}|^2\,\mathrm{B}^{(4)}_{lknk'n'},\end{aligned} \tag{45}$$

where

$$\mathrm{B}^{(1)}_{knk'n'k''} = \mathbb{E}\left\{\left|\sum_{l=1}^{L} a^*_{lkn}\mathbf{g}^H_{lk''}\boldsymbol{\Xi}_{lknk''n'}\mathbf{g}_{lk'}\right|^2\right\}, \tag{46}$$

$$\mathrm{B}^{(2)}_{knk'n'k''} = \mathbb{E}\left\{\left|\sum_{l=1}^{L} a^*_{lkn}\mathbf{g}^H_{lk''}\left(\boldsymbol{\Pi}^T_{k'',\mathrm{t}}\boldsymbol{\Phi}^*_k \otimes \mathbf{I}_M\right)\boldsymbol{\Omega}_{lknn'}\mathbf{g}_{lk'}\right|^2\right\}, \tag{47}$$

$$\mathrm{B}^{(3)}_{lknk'n'} = \mathbb{E}\left\{\left|\left(\boldsymbol{\eta}^{\mathrm{p}}_{l,\mathrm{r}}\right)^H\bar{\boldsymbol{\Omega}}_{lknn'}\mathbf{g}_{lk'}\right|^2\right\}, \tag{48}$$

$$\mathrm{B}^{(4)}_{lknk'n'} = \mathbb{E}\left\{\left|\mathbf{w}^H_l\bar{\boldsymbol{\Omega}}_{lknn'}\mathbf{g}_{lk'}\right|^2\right\} = \sigma^2\operatorname{tr}\left(\bar{\boldsymbol{\Omega}}_{lknn'}\mathbf{R}_{lk'}\bar{\boldsymbol{\Omega}}^H_{lknn'}\right). \tag{49}$$

Corresponding matrices above are defined as $\boldsymbol{\Xi}_{lknk''n'} = (\mathbf{P}^{1/2}_{k''}\bar{\boldsymbol{\Phi}}^*_{k''k} \otimes \mathbf{I}_M)\boldsymbol{\Omega}_{lknn'}$, $\boldsymbol{\Omega}_{lknn'} = \boldsymbol{\Omega}^H_{lkn}\mathbf{S}_{n'}$, $\boldsymbol{\Omega}_{lkn} = \mathbf{D}_{lk}\mathbf{S}_n\boldsymbol{\Psi}_{lk}$, and $\bar{\boldsymbol{\Omega}}_{lknn'} = \left(\boldsymbol{\Phi}^*_k \otimes \mathbf{I}_M\right)\boldsymbol{\Omega}_{lknn'}$, and we need to compute these four parts respectively. Based on Lemma B.14. in [37], $\mathrm{B}^{(1)}_{knk'n'k''}$ is given in (50) at the top of this page. In $\mathrm{B}^{(2)}_{knk'n'k''}$, we can get that $\operatorname{vec}(\boldsymbol{\Pi}^T_{k'',\mathrm{t}}\boldsymbol{\Phi}^*_k) = (\boldsymbol{\Phi}^H_k \otimes \mathbf{I}_N)\operatorname{vec}(\boldsymbol{\Pi}^T_{k'',\mathrm{t}})$, and it follows $\mathcal{CN}\left(\mathbf{0}, (1-\kappa_{\mathrm{t}})\bar{\boldsymbol{\Phi}}_{kk} \otimes \mathbf{P}_{k''}\right)$. Moreover, via (1.11.15) in [56], we observe that $\boldsymbol{\Pi}^T_{k'',\mathrm{t}}\boldsymbol{\Phi}^*_k \otimes \mathbf{I}_M$ is a zero-mean complex Gaussian random matrix, whose covariance matrix is $\mathbf{C}_{kk'',1} = (1-\kappa_{\mathrm{t}})\bar{\boldsymbol{\Phi}}_{kk} \otimes (\mathbf{K}_{MN} \otimes \mathbf{I}_M)(\mathbf{P}_{k''} \otimes (\operatorname{vec}(\mathbf{I}_M)\operatorname{vec}(\mathbf{I}_M)^H))(\mathbf{K}_{NM} \otimes \mathbf{I}_M)$. $\mathbf{K}_{mn} = \sum_{j=1}^{n}\mathbf{e}^T_j \otimes \mathbf{I}_m \otimes \mathbf{e}_j$ is defined as a commutation matrix in [56, Sec. 1.11.1], and $\mathbf{e}_j$ represents the j-th column of $\mathbf{I}_n$. Next, via Lemma 1, 2, and 3, $\mathrm{B}^{(2)}_{knk'n'k''}$ is given in (51) at the top of this page. After that, we rewrite (3), via (1.11.15), (1.11.20), and (1.11.24) in [56], as $\boldsymbol{\eta}^{\mathrm{p}}_{l,\mathrm{r}} = \sqrt{1-\kappa_{\mathrm{r}}}\sum_{k=1}^{K}\left(\bar{\mathbf{P}}^T_k \otimes \mathbf{I}_M\right)\left(\mathbf{E}_2\mathbf{g}_{lk} \odot \breve{\boldsymbol{\eta}}_{lk}\right)$, where $\mathbf{E}_2 = \mathbf{1}^{\tau_p\times 1} \otimes \mathbf{I}_{MN}$, and $\breve{\boldsymbol{\eta}}_{lk} = \operatorname{vec}(\breve{\boldsymbol{\Pi}}_{lk})$ is the vectorized version of the uncorrelated receive distortion. Substituting it into $\mathrm{B}^{(3)}_{lknk'n'}$ and utilizing the independence of $\breve{\boldsymbol{\eta}}_{lk}$ for different index k, $\mathrm{B}^{(3)}_{lknk'n'}$ can be transformed into

$$\begin{aligned}\mathrm{B}^{(3)}_{lknk'n'} &= (1-\kappa_{\mathrm{r}})\sum_{k''=1}^{K}\mathbb{E}\left\{\left\|\bar{\boldsymbol{\Omega}}_{lknk''n'}\mathbf{g}_{lk'} \odot \mathbf{E}_2\mathbf{g}_{lk''}\right\|^2\right\} \\ &= (1-\kappa_{\mathrm{r}})\sum_{k''=1}^{K}\mathrm{B}^{(3)}_{lknk'n'k''},\end{aligned} \tag{52}$$

where $\bar{\boldsymbol{\Omega}}_{lknk''n'} = \bar{\boldsymbol{\Omega}}^H_{lkn,n'}(\bar{\mathbf{P}}^T_{k''} \otimes \mathbf{I}_M)$, and $\mathrm{B}^{(3)}_{lknk'k''n'}$ is further expressed as (53) at the top of the next page via $\mathbb{E}\{\|\mathbf{A}\mathbf{x}\odot\mathbf{B}\mathbf{y}\|^2\} = \operatorname{tr}(\mathbf{A}\mathbf{R}_x\mathbf{A}^H \odot \mathbf{B}\mathbf{R}_y\mathbf{B}^H)$ and $\mathbb{E}\{\|\mathbf{A}\mathbf{x}\odot\mathbf{B}\mathbf{x}\|^2\} = \|\mathbf{A}\mathbf{R}_x\mathbf{B}^H \odot \mathbf{I}_M\|^2 + \operatorname{tr}(\mathbf{A}\mathbf{R}_x\mathbf{A}^H \odot \mathbf{B}\mathbf{R}_x\mathbf{B}^H)$ for $\mathbf{x} \sim \mathcal{CN}(\mathbf{0}, \mathbf{R}_x)$ and $\mathbf{y} \sim \mathcal{CN}\left(\mathbf{0}, \mathbf{R}_y\right)$.

Next, similar to $\mathrm{B}_{knk'n'}$, we decompose $\mathrm{C}_{lknk'n'}$ as

$$\begin{aligned}\mathrm{C}_{lknk'n'} =& \tau_p\kappa_{\mathrm{t}}\kappa_{\mathrm{r}}\sum_{k''=1}^{K}\mathrm{C}^{(1)}_{lknk'n'k''} + \kappa_{\mathrm{r}}\sum_{k''=1}^{K}\mathrm{C}^{(2)}_{lknk'n'k''} \\ &+ \mathrm{C}^{(3)}_{lkn,k'n'} + \mathrm{C}^{(4)}_{lknk'n'}\end{aligned} \tag{54}$$

where

$$\mathrm{C}^{(1)}_{lknk'n'k''} = \mathbb{E}\left\{\|\boldsymbol{\Xi}_{lknk''}\mathbf{g}_{lk''} \odot \mathbf{S}_{n'}\mathbf{g}_{lk'}\|^2\right\}, \tag{55}$$

$$\mathrm{C}^{(2)}_{lknk'n'k''} = \mathbb{E}\left\{\left\|\boldsymbol{\Omega}_{lkn}\left(\boldsymbol{\Phi}^T_k\boldsymbol{\Pi}^*_{k'',\mathrm{t}} \otimes \mathbf{I}_M\right)\mathbf{g}_{lk''} \odot \mathbf{S}_{n'}\mathbf{g}_{lk'}\right\|^2\right\}, \tag{56}$$

$$\mathrm{C}^{(3)}_{lknk'n'} = \mathbb{E}\left\{\left\|\bar{\boldsymbol{\Omega}}_{lkn}\boldsymbol{\eta}^{\mathrm{p}}_{l,\mathrm{r}} \odot \mathbf{S}_{n'}\mathbf{g}_{lk'}\right\|^2\right\}, \tag{57}$$

$$\begin{aligned}\mathrm{C}^{(4)}_{lknk'n'} &= \mathbb{E}\left\{\left\|\bar{\boldsymbol{\Omega}}_{lkn}\mathbf{w}_l \odot \mathbf{S}_{n'}\mathbf{g}_{lk'}\right\|^2\right\} \\ &= \sigma^2\operatorname{tr}\left(\bar{\boldsymbol{\Omega}}_{lkn}\bar{\boldsymbol{\Omega}}^H_{lkn} \odot \mathbf{S}_{n'}\mathbf{R}_{lk'}\mathbf{S}^H_{n'}\right).\end{aligned} \tag{58}$$

Corresponding matrices above are defined as $\boldsymbol{\Xi}_{lknk''} = \boldsymbol{\Omega}_{lkn}(\bar{\boldsymbol{\Phi}}^T_{k''k}\mathbf{P}^{1/2}_{k''} \otimes \mathbf{I}_M)$ and $\bar{\boldsymbol{\Omega}}_{lkn} = \boldsymbol{\Omega}_{lkn}(\boldsymbol{\Phi}^T_k \otimes \mathbf{I}_M)$. Referring to the derivation of $\mathrm{B}^{(3)}_{lknk'n'}$, $\mathrm{C}^{(1)}_{lknk'n'k''}$ is expressed as (59) shown at the top of the next page. Next, we know that $\boldsymbol{\Omega}_{lkn}\left(\boldsymbol{\Phi}^T_k\boldsymbol{\Pi}^*_{k'',\mathrm{t}} \otimes \mathbf{I}_M\right)$ is complex Gaussian, and its covariance can be expressed as $\mathbf{C}_{lknk'',2} = (1-\kappa_{\mathrm{t}})(\mathbf{I}_M \otimes \boldsymbol{\Omega}_{lkn})(\mathbf{P}_{k''} \otimes ((\mathbf{K}_{MN} \otimes \mathbf{I}_M)(\boldsymbol{\Phi}^T_{kk} \otimes \operatorname{vec}(\mathbf{I}_M)\operatorname{vec}(\mathbf{I}_M)^H)(\mathbf{K}_{NM} \otimes \mathbf{I}_M)))(\mathbf{I}_M \otimes \boldsymbol{\Omega}^H_{lkn})$. Based on Lemma 4 and Lemma 5, $\mathrm{C}^{(2)}_{lknk'n'k''}$ is given in (60) at the top of the next page, where $\mathbf{E}_3 = \mathbf{1}^{MN\times MN} \otimes \mathbf{I}_M$. Next, $\mathrm{C}^{(3)}_{lknk'n'}$ can be transformed via $\mathbb{E}\{\|\mathbf{A}(\bar{\mathbf{x}} \odot \mathbf{a}) \odot \mathbf{b}\|^2\} = \|\mathbf{A} \odot \mathbf{b}\mathbf{a}^T\|^2$ for $\bar{\mathbf{x}} \sim \mathcal{CN}(\mathbf{0}, \mathbf{I})$ as

$$\mathrm{B}^{(3)}_{lknk'n'k''} = \mathrm{tr}\left(\bar{\mathbf{\Omega}}_{lknk''n'}\mathbf{R}_{lk'}\bar{\mathbf{\Omega}}^{H}_{lknk''n'} \odot \mathbf{E}_2\mathbf{R}_{lk''}\mathbf{E}_2^H\right) + \begin{cases} 0 & , k'' \neq k' \\ \left\|\bar{\mathbf{\Omega}}_{lknk'n'}\mathbf{R}_{lk'}\mathbf{E}_2^H \odot \mathbf{I}_{MN}\right\|^2 & , k'' = k' \end{cases} \tag{53}$$

$$\mathrm{C}^{(1)}_{lknk'n'k''} = \mathrm{tr}\left(\mathbf{\Xi}_{lknk''}\mathbf{R}_{lk''}\mathbf{\Xi}^{H}_{lknk''} \otimes \mathbf{S}_{n'}\mathbf{R}_{lk'}\mathbf{S}_{n'}^H\right) + \begin{cases} 0 & , k'' \neq k' \\ \left\|\mathbf{S}_{n'}\mathbf{R}_{lk'}\mathbf{\Xi}^{H}_{lknk'} \odot \mathbf{I}_{M}\right\|^2 & , k'' = k' \end{cases} \tag{59}$$

$$\mathrm{C}^{(2)}_{lknk'n'k''} = \mathrm{tr}\left(\left(\mathbf{R}_{lk''} \otimes \left(\mathbf{S}_{n'}\mathbf{R}_{lk'}\mathbf{S}_{n'}^H \odot \mathbf{I}_M\right)\right)\mathbf{C}^{T}_{lknk'',2}\right) + \begin{cases} 0 & , k'' \neq k' \\ \mathrm{vec}\left(\mathbf{S}_{n'}\mathbf{R}_{lk'}\right)^H\left(\mathbf{C}_{lknk',2} \odot \mathbf{E}_3\right)\mathrm{vec}\left(\mathbf{S}_{n'}\mathbf{R}_{lk'}\right) & , k'' = k' \end{cases} \tag{60}$$

$$\mathrm{C}^{(3)}_{lknk'n'k''} = \mathrm{tr}\left(\bar{\mathbf{\Omega}}_{lknk''}\left(\mathbf{E}_2\mathbf{R}_{lk''}\mathbf{E}_2^H \odot \mathbf{I}_{\tau_p MN}\right)\bar{\mathbf{\Omega}}^{H}_{lknk''} \odot \mathbf{S}_{n'}\mathbf{R}_{lk'}\mathbf{S}_{n'}^H\right) + \begin{cases} 0 & , k'' \neq k' \\ \left\|\bar{\mathbf{\Omega}}_{lknk'} \odot \mathbf{S}_{n'}\mathbf{R}_{lk'}\mathbf{E}_2^H\right\|^2 & , k'' = k' \end{cases} \tag{62}$$

$$\begin{aligned} \mathrm{C}^{(3)}_{lknk'n'} &= (1-\kappa_{\mathrm{r}})\sum_{k''=1}^{K}\mathbb{E}\left\{\left\|\bar{\mathbf{\Omega}}_{lknk''} \odot \mathbf{S}_{n'}\mathbf{g}_{lk'}\mathbf{g}^{T}_{lk''}\mathbf{E}_2^T\right\|^2\right\} \\ &= (1-\kappa_{\mathrm{r}})\sum_{k''=1}^{K}\mathrm{C}^{(3)}_{lknk'n'k''}, \end{aligned} \tag{61}$$

where $\bar{\mathbf{\Omega}}_{lknk''} = \bar{\mathbf{\Omega}}_{lkn}\left(\bar{\mathbf{P}}^{T}_{k''} \otimes \mathbf{I}_M\right)$. The rest part in (61) can be computed as (62) at the top of this page via $\mathbb{E}\{\|\mathbf{C} \odot \mathbf{A}\mathbf{x}\mathbf{y}^T\mathbf{B}^T\|^2\} = \mathrm{tr}(\mathbf{A}\mathbf{R}_x\mathbf{A}^H \odot \mathbf{C}(\mathbf{B}\mathbf{R}_y\mathbf{B}^H \odot \mathbf{I}_M)\mathbf{C}^H)$ and $\mathbb{E}\{\|\mathbf{C} \odot \mathbf{A}\mathbf{x}\mathbf{x}^T\mathbf{B}^T\|^2\} = \|\mathbf{C} \odot \mathbf{A}\mathbf{R}_x\mathbf{B}^H\|^2 + \mathrm{tr}(\mathbf{A}\mathbf{R}_x\mathbf{A}^H \odot \mathbf{C}(\mathbf{B}\mathbf{R}_x\mathbf{B}^H \odot \mathbf{I}_M)\mathbf{C}^H)$ for $\mathbf{x} \sim \mathcal{CN}(\mathbf{0}, \mathbf{R}_x)$ and $\mathbf{y} \sim \mathcal{CN}(\mathbf{0}, \mathbf{R}_y)$. In the end, combining all the parts and transforming them into the matrix version, we can obtain (13).

Appendix C
Proof of Theorem 3

For simplicity, we let $\mathbf{D}_{lk} = \mathbf{I}_M$. First, it is easy to get $\mathbb{E}\{\mathbf{V}_{lk}^H\mathbf{G}_{lk}\} = \mathbb{E}\{\mathbf{V}_{lk}^H\mathbf{V}_{lk}\} = \mathbf{B}_{lk}$, and thereafter $\mathbb{E}\{\mathbf{Q}_{kk}\}$ and the first term in $\mathbf{\Theta}_{lk}$ can be derived as $\mathbf{Q}_k$ and $\mathbf{S}_k$. Then, we compute the second term in $\mathbf{\Theta}_{lk}$ via the approximate method mentioned in advance. In terms of $\mathbf{a}^H\left(\mathbf{I} \odot \mathbf{b}\mathbf{b}^H\right)\mathbf{c} = \mathrm{tr}(\mathbf{c}\mathbf{a}^H \odot \mathbf{b}\mathbf{b}^H)$, we have $\mathbb{E}\{\mathbf{V}_{lk}^H(\sum_{k'=1}^{K}\mathbf{G}_{lk'}\mathbf{P}_{k'}\mathbf{G}_{lk'}^H \odot \mathbf{I}_M)\mathbf{V}_{lk}\} \approx \mathbf{T}_{lk}$.

Next, we notice that the submatrix $\bar{\mathbf{Q}}_{kk',mn}$ can be easily obtained due to the independence between index m and n when $m \neq n$. For $m = n$, we extract $\mathbf{P}_k$ from $\bar{\mathbf{Q}}_{kk',m} = \mathbb{E}\{\hat{\mathbf{G}}_{mk}^H\mathbf{G}_{mk'}\mathbf{P}_k\mathbf{G}_{mk'}^H\hat{\mathbf{G}}_{mk}\}$ and compute each element. The proof of $\mathbb{E}\{\mathbf{Q}_{kk'}\mathbf{P}_{k'}\mathbf{Q}_{kk'}^H\} = \bar{\mathbf{Q}}_{kk'}$ is comparable to the proof of $\mathrm{B}_{lkn,k'n'}$ in Appendix B and is thereby omitted. Finally, combining all the terms and utilizing $\det(\mathbf{I}+\mathbf{A}\mathbf{B}) = \det(\mathbf{I}+\mathbf{B}\mathbf{A})$, (26) can be obtained.

References

[1] M. Xie, X. Yu, J. Xu, and X. D, "Low-complexity channel estimation scheme for cell-free massive MIMO with hardware impairment," in *Proc. IEEE Global Commun. Conf. (GLOBECOM)*, Dec. 2022, pp. 711-716.

[2] D. Ciuonzo, P. S. Rossi, and S. Dey, "Massive MIMO channel-aware decision fusion," *IEEE Trans. Signal Process.*, vol. 63, no. 3, pp. 604-619, Feb. 2015.

[3] A. S. Bana, et al., " Massive MIMO for Internet of Things (IoT) connectivity," *Physical Commun.*, vol. 37, no. 100859, Sep. 2019.

[4] I. Dey, D. Ciuonzo, and P. S. Rossi, "Wideband collaborative spectrum sensing using massive MIMO decision fusion," *IEEE Trans. Wireless Commun.*, vol. 19, no. 8, pp. 5246-5260, Aug. 2020.

[5] B. Yang, Z. Yu, J. Lan, R. Zhang, J. Zhou, and W. Hong, "Digital beamforming-based massive MIMO transceiver for 5G millimeter-wave communications," *IEEE Trans. Microw. Theory Techn.*, vol. 66, no. 7, pp. 3403-3418, July 2018.

[6] M. Chung, L. Liu, O. Edfors, and F. Tufvesson, "Demo: Millimeter-wave massive MIMO testbed with hybrid beamforming," in *Proc. IEEE Wireless Commun. Netw. Conf. Workshops (WCNCW)*, Apr. 2020, pp. 1-2.

[7] Y. Hu, J. Zhan, Z. H. Jiang, C. Yu, and W. Hong, "An orthogonal hybrid analog–digital multibeam antenna array for millimeter-wave massive MIMO systems," *IEEE Trans. Antennas Propag.*, vol. 69, no. 3, pp. 1393-1403, March 2021.

[8] T. V. Chien, H. Q. Ngo, S. Chatzinotas, and B. Ottersten, "Reconfigurable intelligent surface-assisted massive MIMO: Favorable propagation, channel hardening, and rank deficiency [Lecture notes]," *IEEE Signal Process. Mag.*, vol. 39, no. 3, pp. 97-104, May 2022.

[9] A. Liu et al., "A survey on fundamental limits of integrated sensing and communication," *IEEE Commun. Surveys Tut.*, vol. 24, no. 2, pp. 994-1034, 2nd Quart. 2022.

[10] Y. G. Lim, C. B. Chae, and G. Caire, "Performance analysis of massive MIMO for cell-boundary users," *IEEE Trans. Wireless Commun.*, vol. 14, no. 12, pp. 6827-6842, Dec. 2015.

[11] J. Zhang, E. Björnson, M. Matthaiou, D. W. K. Ng, H. Yang, and D. J. Love, "Prospective multiple antenna technologies for beyond 5G," *IEEE J. Sel. Areas Commun.*, vol. 38, no. 8, pp. 1637-1660, Aug. 2020.

[12] G. Interdonato, E. Björnson, H. Q. Ngo, P. Frenger, and E. G. Larsson, "Ubiquitous cell-free massive MIMO communications," *EURASIP J. Wireless Commun. Netw.*, vol. 2019, no. 197, 2019.

[13] H. Q. Ngo, A. Ashikhmin, H. Yang, E. G. Larsson, and T. L. Marzetta, "Cell-free massive MIMO versus small cells," *IEEE Trans. Wireless Commun.*, vol. 16, no. 3, pp. 1834-1850, March 2017.

[14] H. Q. Ngo, L. N. Tran, T. Q. Duong, M. Matthaiou, and E. G. Larsson, "On the total energy efficiency of cell-free massive MIMO," *IEEE Trans. Green Commun. Netw.*, vol. 2, no. 1, pp. 25-39, March 2018.

[15] S. Buzzi and C. D' Andrea, "Cell-free massive MIMO: User-centric approach," *IEEE Wireless Commun. Lett.*, vol. 6, no. 6, pp. 706-709, Dec. 2017.

[16] E. Björnson and L. Sanguinetti, "Scalable cell-free massive MIMO systems," *IEEE Trans. Commun.*, vol. 68, no. 7, pp. 4247-4261, July 2020.

[17] Z. Chen and E. Björnson, "Channel hardening and favorable propagation in cell-free massive MIMO with stochastic geometry," *IEEE Trans. Commun.*, vol. 66, no. 11, pp. 5205-5219, Nov. 2018.

[18] A. Adhikary, A. Ashikhmin, and T. L. Marzetta, "Uplink interference reduction in large-scale antenna systems," *IEEE Trans. Commun.*, vol. 65, no. 5, pp. 2194-2206, May 2017.

[19] E. Björnson and L. Sanguinetti, "Making cell-free massive MIMO competitive with MMSE processing and centralized implementation," *IEEE Trans. Wireless Commun.*, vol. 19, no. 1, pp. 77-90, Jan. 2020.

[20] Ö. Özdogan, E. Björnson, and J. Zhang, "Performance of cell-free massive MIMO with rician fading and phase shifts," *IEEE Trans. Wireless Commun.*, vol. 18, no. 11, pp. 5299-5315, Nov. 2019.

[21] Z. Wang, J. Zhang, E. Björnson, and B. Ai, "Uplink performance of cell-free massive MIMO over spatially correlated rician fading channels," *IEEE Commun. Lett.*, vol. 25, no. 4, pp. 1348-1352, April 2021.

[22] X. Li, E. Björnson, S. Zhou, and J. Wang, "Massive MIMO with multi-antenna users: When are additional user antennas beneficial?" in *Proc. 23rd Int. Conf. Telecommun. (ICT)*, pp. 1-6, May 2016.

[23] K. Dovelos, M. Matthaiou, H. Q. Ngo, and B. Bellalta, "Massive MIMO with multi-antenna users under jointly correlated Ricean fading," in *Proc. IEEE Int. Conf. Commun. (ICC)*, Jun. 2020, pp. 1-6.

[24] J. A. C. Sutton, H. Q. Ngo, and M. Matthaiou, "Hardening the channels by precoder design in massive MIMO with multiple-antenna users," *IEEE Trans. Veh. Technol.*, vol. 70, no. 5, pp. 4541-4556, May 2021.

[25] M. Alonzo, S. Buzzi, A. Zappone, and C. D' Elia, "Energy-efficient power control in cell-free and user-centric massive MIMO at millimeter wave," *IEEE Trans. Green Commun. Netw.*, vol. 3, no. 3, pp. 651-663, Sept. 2019.

[26] T. C. Mai, H. Q. Ngo, and T. Q. Duong, "Uplink spectral efficiency of cell-free massive MIMO with multi-antenna users," in *Proc. 3rd Int. Conf. Recent Adv. Signal Process. Telecommun. Comput. (SigTelCom)*, pp. 126-129, Mar. 2019.

[27] S. Buzzi, C. D' Andrea, A. Zappone, and C. D' Elia, "User-centric 5G cellular networks: Resource allocation and comparison with the cell-free massive MIMO approach," *IEEE Trans. Wireless Commun.*, vol. 19, no. 2, pp. 1250-1264, Feb. 2020.

[28] T. C. Mai, H. Q. Ngo, and T. Q. Duong, "Downlink spectral efficiency of cell-free massive MIMO systems with multi-antenna users," *IEEE Trans. Commun.*, vol. 68, no. 8, pp. 4803-4815, Aug. 2020.

[29] M. Zhou, L. Yang, and H. Zhu, "Sum-SE for multigroup multicast cell-free massive MIMO with multi-antenna users and low-resolution DACs," *IEEE Wireless Commun. Lett.*, vol. 10, no. 8, pp. 1702-1706, Aug. 2021.

[30] M. Zhou, Y. Zhang, X. Qiao, M. Xie, L. Yang, and H. Zhu, "Multigroup multicast downlink cell-free massive MIMO systems with multiantenna users and low-resolution ADCs/DACs," *IEEE Sys. J.*, vol. 16, no. 3, pp. 3578-3589, Sept. 2022.

[31] Z. Wang, J. Zhang, B. Ai, C. Yuen, and M. Debbah, "Uplink performance of cell-free massive MIMO with multi-antenna users over jointly-correlated rayleigh fading channels," *IEEE Trans. Wireless Commun.*, vol. 21, no. 9, pp. 7391-7406, Sept. 2022.

[32] X. Li, J. Zhang, Z. Wang, B. Ai, and D. W. K. Ng, "Cell-free massive MIMO with multi-antenna users over weichselberger Rician channels," *IEEE Trans. Veh. Technol.*, vol. 71, no. 11, pp. 12368-12373, Nov. 2022.

[33] S. Jacobsson, G. Durisi, M. Coldrey, T. Goldstein, and C. Studer, "Quantized precoding for massive MU-MIMO," *IEEE Trans. Commun.*, vol. 65, no. 11, pp. 4670-4684, Nov. 2017.

[34] E. Björnson, L. Sanguinetti, and J. Hoydis, "Hardware distortion correlation has negligible impact on UL massive MIMO spectral efficiency," *IEEE Trans. Commun.*, vol. 67, no. 2, pp. 1085-1098, Feb. 2019.

[35] E. Björnson, J. Hoydis, M. Kountouris, and M. Debbah, "Massive MIMO systems with non-ideal hardware: Energy efficiency, estimation, and capacity limits," *IEEE Trans. Inform. Theory*, vol. 60, no. 11, pp. 7112-7139, Nov. 2014.

[36] E. Björnson, M. Matthaiou, and M. Debbah, "Massive MIMO with non-ideal arbitrary arrays: Hardware scaling laws and circuit-aware design," *IEEE Trans. Wireless Commun.*, vol. 14, no. 8, pp. 4353-4368, Aug. 2015.

[37] E. Björnson, J. Hoydis, and L. Sanguinetti, "Massive MIMO networks: Spectral, energy, and hardware efficiency," *Found. Trends Signal Process.*, vol. 11, no. 3-4, pp. 154-655, 2017.

[38] J. Zhang, Y. Wei, E. Björnson, Y. Han, and S. Jin, "Performance analysis and power control of cell-free massive MIMO systems with hardware impairments," *IEEE Access*, vol. 6, pp. 55302-55314, 2018.

[39] J. Zheng, J. Zhang, L. Zhang, X. Zhang, and B. Ai, "Efficient receiver design for uplink cell-free massive MIMO with hardware impairments," *IEEE Trans. Veh. Technol.*, vol. 69, no. 4, pp. 4537-4541, April 2020.

[40] X. Hu, C. Zhong, X. Chen, W. Xu, H. Lin, and Z. Zhang, "Cell-free massive MIMO systems with low resolution ADCs," *IEEE Trans. Commun.*, vol. 67, no. 10, pp. 6844-6857, Oct. 2019.

[41] Y. Zhang, L. Yang, and H. Zhu, "Cell-free massive MIMO systems with low-resolution ADCs: The rician fading case," *IEEE Sys. J.*, vol. 16, no. 1, pp. 1471-1482, March 2022.

[42] H. Masoumi and M. J. Emadi, "Performance analysis of cell-free massive MIMO system with limited fronthaul capacity and hardware impairments," *IEEE Trans. Wireless Commun.*, vol. 19, no. 2, pp. 1038-1053, Feb. 2020.

[43] Z. Mokhtari and R. Dinis, "Sum-rate of cell free massive MIMO systems with power amplifier non-linearity," *IEEE Access*, vol. 9, pp. 141927-141937, 2021.

[44] A. Papazafeiropoulos, E. Björnson, P. Kourtessis, S. Chatzinotas, and J. M. Senior, "Scalable cell-free massive MIMO systems: Impact of hardware impairments," *IEEE Trans. Veh. Technol.*, vol. 70, no. 10, pp. 9701-9715, Oct. 2021.

[45] P. Kuo, H. T. Kung, and P. Ting, "Compressive sensing based channel feedback protocols for spatially-correlated massive antenna arrays," in *Proc. IEEE Wireless Commun. Netw. Conf. (WCNC)*, Apr. 2012, pp. 492-497.

[46] D. Tse and P. Viswanath, *Fundamentals of wireless communication*. Cambridge, U.K.: Cambridge Univ. Press, 2005.

[47] Ö. T. Demir, E. Björnson, and L. Sanguinetti, "Foundations of user-centric cell-free massive MIMO," *Found. Trends Signal Process.*, vol. 14, no. 3-4, pp. 162-472, 2021.

[48] E. Björnson, L. Sanguinetti, and M. Debbah, "Massive MIMO with imperfect channel covariance information," in *Proc. 50th Asilomar Conf. Signals Syst. Comput.* 2016, pp. 974–978.

[49] S. Haghighatshoar and G. Caire, "Massive MIMO pilot decontamination and channel interpolation via wideband sparse channel estimation," *IEEE Trans. Wireless Commun.*, vol. 16, no. 12, pp. 8316-8332, Dec. 2017.

[50] D. Neumann, M. Joham, and W. Utschick, "Covariance matrix estimation in massive MIMO," *IEEE Signal Process. Lett.*, vol. 25, no. 6, pp. 863-867, June 2018.

[51] K. Upadhya and S. A. Vorobyov, "Covariance matrix estimation for massive MIMO," *IEEE Signal Process. Lett.*, vol. 25, no. 4, pp. 546-550, April 2018.

[52] L. Sanguinetti, E. Björnson, and J. Hoydis, "Toward massive MIMO 2.0: Understanding spatial correlation, interference suppression, and pilot contamination," *IEEE Trans. Commun.*, vol. 68, no. 1, pp. 232-257, Jan. 2020.

[53] Ö. T. Demir and E. Björnson, "The Bussgang decomposition of nonlinear systems: Basic theory and MIMO extensions [Lecture notes]," *IEEE Signal Process. Mag.*, vol. 38, no. 1, pp. 131-136, Jan. 2021.

[54] D. Verenzuela, E. Björnson, and L. Sanguinetti, "Spectral and energy efficiency of superimposed pilots in uplink massive MIMO," *IEEE Trans. Wireless Commun.*, vol. 17, no. 11, pp. 7099-7115, Nov. 2018.

[55] S. Chen, J. Zhang, E. Björnson, J. Zhang, and B. Ai, "Structured massive access for scalable cell-free massive MIMO systems," *IEEE J. Sel. Areas Commun.*, vol. 39, no. 4, pp. 1086-1100, April 2021.

[56] X. Zhang, *Matrix analysis and applications*. Cambridge, U.K.: Cambridge Univ. Press, 2017.